JOURNAL OF GEOPHYSICAL RESEARCH, VOL. 114, A04308, doi:10.1029/2008JA013749, 2009

Conjugate Point Equatorial Experiment (COPEX) campaign in Brazil: Electrodynamics highlights on spread *F* development conditions and day-to-day variability

M. A. Abdu,[1] I. S. Batista,[1] B. W. Reinisch,[2] J. R. de Souza,[1] J. H. A. Sobral,[1] T. R. Pedersen,[3] A. F. Medeiros,[4] N. J. Schuch,[5] E. R. de Paula,[1] and K. M. Groves[3]

Received 13 September 2008; revised 21 November 2008; accepted 6 January 2009; published 9 April 2009.

[1] A Conjugate Point Equatorial Experiment (COPEX) campaign was conducted during the October–December 2002 period in Brazil, with the objective to investigate the equatorial spread *F*/plasma bubble irregularity (ESF) development conditions in terms of the electrodynamical state of the ionosphere along the magnetic flux tubes in which they occur. A network of instruments, including Digisondes, optical imagers, and GPS receivers, was deployed at magnetic conjugate and dip equatorial locations in a geometry that permitted field line mapping of the conjugate *E* layers to dip equatorial *F* layer bottomside. We analyze in this paper the extensive Digisonde data from the COPEX stations, complemented by limited all-sky imager conjugate point observations. The Sheffield University Plasmasphere-Ionosphere Model (SUPIM) is used to assess the transequatorial winds (TEW) as inferred from the observed difference of h_mF_2 at the conjugate sites. New results and evidence on the ESF development conditions and the related ambient electrodynamic processes from this study can be highlighted as follows: (1) large-scale bottomside wave structures/satellite traces at the equator followed by their simultaneous appearance at conjugate sites are shown to be indicative of the ESF instability initiation; (2) the evening prereversal electric field enhancement (PRE)/vertical drift presents systematic control on the time delay in SF onset at off-equatorial sites indicative of the vertical bubble growth, under weak transequatorial wind; (3) the PRE presents a large latitude/height gradient in the Brazilian sector; (4) conjugate point symmetry/asymmetry of large-scale plasma depletions versus smaller-scale structures is revealed; and (5) while transequatorial winds seem to suppress ESF development in a case study, the medium-term trend in the ESF seems to be controlled more by the variation in the PRE than in the TEW during the COPEX period. Competing influences of the evening vertical plasma drift in favoring the ESF development and that of the TEW in suppressing its growth are discussed, presenting a perspective on the ESF day-to-day and medium-term variabilities.

Citation: Abdu, M. A., I. S. Batista, B. W. Reinisch, J. R. de Souza, J. H. A. Sobral, T. R. Pedersen, A. F. Medeiros, N. J. Schuch, E. R. de Paula, and K. M. Groves (2009), Conjugate Point Equatorial Experiment (COPEX) campaign in Brazil: Electrodynamics highlights on spread *F* development conditions and day-to-day variability, *J. Geophys. Res.*, *114*, A04308, doi:10.1029/2008JA013749.

1. Introduction

[2] Equatorial spread *F*/plasma bubble irregularities (ESF) development occurs under unique electrodynamical conditions of the ionosphere near sunset. The rapid uplift of the evening equatorial *F* layer is driven by an enhancement in the eastward electric field, widely known as the prereversal electric field enhancement (PRE), that arises from the dominating role of an *F* layer dynamo. The bottomside positive gradient region of the rapidly rising *F* layer becomes unstable to density perturbations leading to the growth of plasma depleted flux tubes/plasma bubbles. A widely recognized fact is that the plasma bubbles are basically driven by the Rayleigh-Taylor interchange instability mechanism, operating on a "seed perturbation" at the bottomside density gradient region, and the lower-density plasma of the *F* layer bottomside rises to the topside ionosphere in field-aligned structures, under the action of strong polarization electric fields of the developing bubbles, as inferred directly or indirectly from measurements by different

[1]Instituto Nacional de Pesquisas Espaciais, São José dos Campos, Brazil.
[2]Center for Atmospheric Research, University of Massachusetts, Lowell, Massachusetts, USA.
[3]Air Force Research Laboratory, Hanscom Air Force Base, Massachusetts, USA.
[4]Departamento de Física, Universidade Federal de Campina Grande, Campina Grande, Brazil.
[5]Centro Regional Sul de Pesquisas Espaciais, INPE, Santa Maria, Brazil.

0148-0227/09/2008JA013749$09.00

techniques [*Hanson and Sanatani*, 1973; *Woodman and LaHoz*, 1976; *Tsunoda*, 1981; *Abdu et al.*, 1983a; *Kelley*, 1989; *Fejer et al.*, 1999]. The steep density gradient regions of the developing bubbles being conducive to the growth of secondary instabilities leads to a cascading process resulting in the formation of a wide spectrum of irregularities with scales sizes ranging from tens of centimeters to tens of kilometers [*Haerendel et al.*, 1992]. Thus in a flux tube–aligned configuration the ESF structures extend in latitude depending upon their vertical growth/development above the dip equator. On the basis of the presently known theoretical and model simulation studies [e.g., *Zalesak et al.*, 1982; *Sultan*, 1996; *Keskinen et al.*, 2003] (see also *Abdu* [2001] for a review) the following interdependent factors of the ambient ionosphere-thermosphere system control such vertical growth: (1) the evening *F* layer height and the vertical plasma drift due to the prereversal electric field enhancement (PRE) [*Farley et al.*, 1970; *Abdu et al.*, 1983b; *Fejer et al.*, 1999] that are controlled by the thermospheric zonal wind (eastward in the evening) and the longitudinal/local time gradient in the integrated *E* layer conductivity near sunset [*Rishbeth*, 1971; *Heelis et al.*, 1974], (2) development of a steep density gradient at the *F* layer bottomside where instability is initiated by seed perturbations (widely believed to be arising from gravity waves [see, e.g., *Fritts et al.*, 2008; *Abdu et al.*, 2009]), (3) the integrated Pedersen conductivity of the unstable flux tube which is controlled by thermospheric meridional/transequatorial winds, represented also by the symmetry/asymmetry conditions of the equatorial ionization anomaly (EIA) as proposed by *Maruyama* [1988] and observationally investigated by various authors [e.g., *Valladares et al.*, 2001; *Mendillo et al.*, 2001; *Abdu et al.*, 2006b; *Saito and Maruyama*, 2006; *Thampi et al.*, 2006]. *Sekar and Raghavarao* [1995] have shown that the topside bubble growth and the zonal and vertical extents are dependent also on the background plasma densities and hence on the topside density gradients. The possible influence of a meridional wind from Equatorial Temperature and Wind Anomaly (ETWA) in the development of bottomside spread *F* has been discussed by *Devasia et al.* [2002] and *Jyoti et al.* [2004]. The postsunset ESF occurrence is known to undergo variabilities at short-term, day-to-day, medium-term and long-term scales. The long-term variation pattern is known to depend largely on the solar flux intensity. Its seasonal variation which is longitude dependent is understood in terms of the solar declination and the alignment of the solar terminator with magnetic meridian, i.e., the longitude-dependent magnetic declination angle [*Abdu et al.*, 1981b; *Tsunoda*, 1985; *Kil and Heelis*, 1998; *Burke et al.*, 2004; *Su et al.*, 2008].

[3] The pattern and causes of the ESF short-term and day-to-day variabilities, on the other hand, remain the least understood aspect of the ESF phenomenon. A better understanding of the nature of such variabilities is an important requirement toward developing any predictive capability on the ESF occurrence conditions. One aspect of the ESF variability appears to be interwoven in its relationship with the EIA [see, e.g., *Sridharan et al.*, 1994; *Raghavarao et al.*, 1988; *Abdu*, 2001], while the broader question involves detailed analysis on the complex and competing roles of the above mentioned items 1–3 in the ESF development. An important source of the ESF variability resides in what appears to be inherent in the nature of the seeding mechanism. In this respect it is under debate whether the seeding mechanism originates from a remote gravity wave source and/or local instability growth by other processes such as, for example, the wind driven instability of the bottomside *F* layer to serve as seed perturbation to topside bubble development, as proposed by *Kudeki et al.* [2007], or the velocity shear mechanism at the *F* layer bottomside as proposed by *Hysell and Kudeki* [2004]. The possibility of ESF initiation by electric field perturbation due to gravity waves winds in the *E* region has been discussed by *Prakash* [1999]. Also under discussion is the possible role of a sporadic *E* layer instability mechanism for initiating the conditions for ESF development [*Tsunoda*, 2007; *Cosgrove and Tsunoda*, 2002]. More recently an important source of the ESF day-to-day variability has been shown to arise from planetary wave modulation of the evening prereversal enhancement in the zonal electric field (PRE)/vertical plasma drift [*Abdu et al.*, 2006c]. Ionosphere-magnetosphere coupling processes under magnetically disturbed conditions are also known to be an important source of the ESF variability [*Sastri et al.*, 1997; *Abdu*, 1997; *Abdu et al.*, 2003]. A better understanding of the nature and causes of the variabilities in the ambient ionospheric electrodynamical parameters is a necessary requirement for further progress in this area. Motivated by the need to improve our understanding of the ESF day-to-day variability as related to some of the above factors, a Conjugate Point Equatorial Experiment (COPEX) campaign of approximately 2-month duration was conducted in Brazil during the October–December period of 2002. Data were collected on the vertical distribution of ionospheric electron density by Digisonde Portable Sounders (DPS-4s), airglow imageries using all-sky imagers, and GPS receivers for total electron content and *L* band scintillation and irregularity zonal drift measurements.

[4] This paper discusses the spread *F* development and the related symmetry/asymmetry conditions of the ambient ionospheric and electrodynamic parameters by analyzing the data from the equatorial and conjugate sites. The parameters analyzed include the signatures of the ESF in ionograms and of plasma density depletions in airglow all-sky imagers, the *F* layer electron density height distributions through their defining/critical parameters, h_mF_2 and f_oF_2, and the evening *F* region vertical plasma drifts at the equatorial and conjugate sites, The conjugate point difference in *F* layer peak heights and the vertical drifts are used to infer the cross equatorial/meridional thermospheric winds and their day-to-day variability. The Sheffield University Plasmasphere-Ionosphere Model (SUPIM) [*Bailey and Balan*, 1996] is used to evaluate the transequatorial winds in terms of the hemispheric asymmetry in the EIA, that is, in terms of the conjugate point *F* layer peak heights, in this case. The overall analysis seeks to achieve a better understanding, and clarifications, on some major outstanding questions concerning the ESF onset and development characteristics, such as the role of large-scale wave structures over the equator as precursor to spread *F* development, large- and medium-scale plasma irregularity structures and their conjugate point symmetry/asymmetry conditions, requirement of the evening prereversal enhancement in vertical drift for

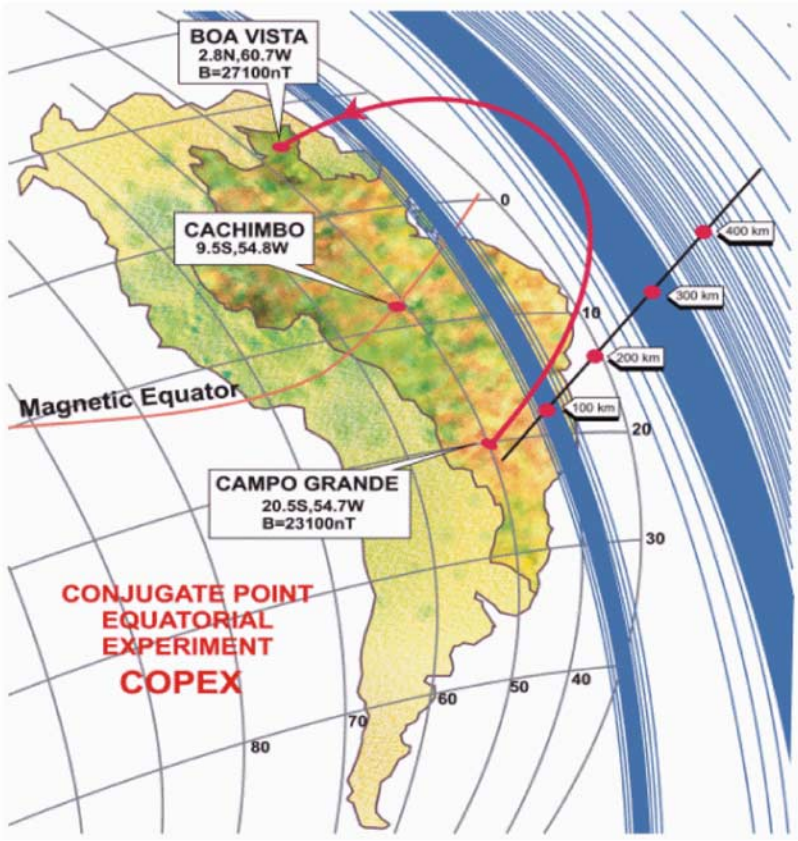

Figure 1a. A schematic of the COPEX geometry showing the magnetic field line connection between the conjugate *E* layers and the equatorial *F* layer peak/bottomside.

different conditions of bubble development (inferred by the differences in the observed time delays for spread *F* over off-equatorial sites), the role of the evening vertical drift in the ESF development as against the role of a transequatorial wind in suppressing such development, etc. Data are analyzed for magnetically quiet conditions and in the context of the relative roles of the different ambient parameters in influencing the spread *F* irregularity developments, and its day-to-day variability.

2. Experimental Setup

[5] The observing stations were located such that the conjugate *E* layers are field line mapped to the *F* layer peak, or to the *F* layer bottomside, over the magnetic equator, a geometry that can help investigate the possible effects on the bubble development process arising from changes in the field line integrated conductivity with associated changes in meridional/transequatorial winds. From the sketch of the magnetic field line station geometry presented in Figure 1a we note that the Brazilian territory in its central longitude region satisfies the required magnetic conjugacy conditions. The three selected locations are as follows: Campo Grande (CG), 20°26′34″S; 54°38′47″W; dip: −22°19′ (southern conjugate point); Boa Vista (BV): 02°49′11″N, 60°40′24″W; dip: 22° (northern conjugate point); and Cachimbo (CX): 9°28′00″S, 54°50′00″W; dip: −4°15′ (near the magnetic equator). We may note that the conjugate sites are somewhat equatorward of the Equatorial Ionization Anomaly (EIA) crest latitude which is nominally at ±15°–18° (dip angle: ±30°–36°). The map in Figure 1b shows the geographic locations of the stations as well as the magnetic inclination and declination characteristics of the Brazilian region as specified in Table 1. Table 2 lists the network of instruments deployed at the different sites during the COPEX campaign, although the results to be presented here are based on the data source from a subset of the instruments consisting mainly of the DPS-4 sounders and the 630 nm all-sky imagers. The data collection by the DPS-4 [*Reinisch*, 1996] was at a cadence of 5 min during the night and 10 min during the day. The all-sky imaging data were collected at 5-min intervals. Except for a few days of interruption over Boa Vista the Digisonde data for all the stations covered all common days of the campaign interval that extended from the day 278 (5 October) to the day 344 (10 December) of the year 2002.

3. Presentation of the Results

[6] Some preliminary COPEX campaign results have previously been published and presented [e.g., *Abdu et al.*, 2004; *Reinisch et al.*, 2004]. The present paper and a companion paper by *Sobral et al.* [2009] use the conjugate point Digisonde and all-sky optical imager data to address issues related to (1) conjugate point ionospheric symmetry/asymmetry conditions related to the ESF mentioned in section 1 and (2) zonal plasma bubble irregularity drift velocities as obtained from the optical imageries and GPS spaced scintillation receivers and their theoretical evaluations, respectively, while the other COPEX results pub-

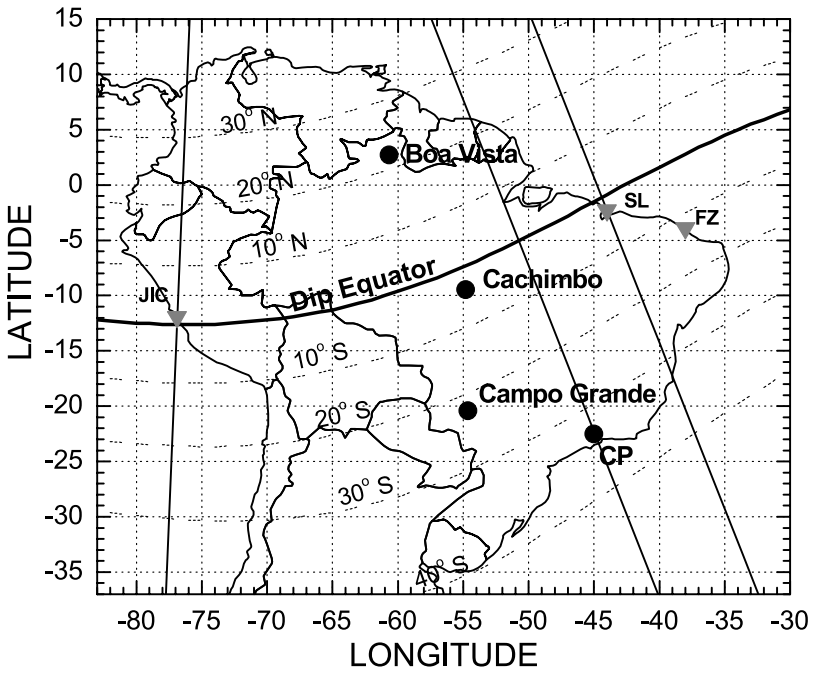

Figure 1b. COPEX campaign station sites, Boa Vista, northern conjugate point; Campo Grande, southern conjugate point; and Cachimbo close to the magnetic equator. Also included are the locations of the permanent ionosonde stations in Brazil, Sao Luis, Fortaleza, and Cachoeira Paulista and Jicamarca in Peru.

lished more recently elsewhere concern, first, field line integrated conductivity effects as related to the connection between spread *F* development and E_s layers at conjugate locations [*Batista et al.*, 2008], second, F_2 peak parameters, drifts and spread *F* derived from Digisonde ionograms for the COPEX Campaign in Brazil [*McNamara et al.*, 2008], and, third, GPS *L* band scintillations and ionospheric irregularity zonal drifts inferred at equatorial and low-latitude regions [*Muella et al.*, 2008]. This paper, concentrating on item 1 above, is organized as follows: section 3.1 covers the general characteristics of the ESF irregularities at conjugate locations, section 3.2 covers evening vertical plasma drift (zonal electric field) and ESF development, section 3.3 covers symmetry/asymmetry in h_mF_2 and transequatorial winds (TEW), section 3.4 covers transequatorial winds and ESF, section 3.5 covers the medium-term trend in the transequatorial wind and evening vertical drift, section 4 is the discussion, and section 5 presents the conclusions.

3.1. General Characteristics of the ESF Irregularities at the Conjugate Locations

[7] The general characteristics of the ESF irregularities have been dealt with extensively by, for example, *Rastogi* [1980], *Abdu et al.* [1981a], *Kil and Heelis* [1998], and *Su et al.* [2008]. Figure 2 shows the spread *F* initiation sequence at the three COPEX stations on the evening of 9 October 2002. The spread *F* onsets are marked by the appearance of oblique (off-vertical) traces (indicated by arrows) adjacent to the main *F* layer trace, indicating "large-scale" wave structures in the bottomside electron density distribution. Their evolution into range-spread echo traces is captured with 5-min resolution at all the three stations. The wave structure (or its indication) first appears over Cachimbo (near the magnetic equator) in the ionogram at 2205 UT (1825 LT), which corresponds to an echo source located immediately west of the station (on the basis of the virtual range and the echo location color code of the ionogram). Over the conjugate sites the first wave structure appears around 2245 UT/1905 LT (almost simultaneously within the uncertainty of the 5-min observation cadence), close to the northeast direction, by which time the trace over Cachimbo had evolved into a typical bottomside range spread structure (not shown here). The appearance of the first traces at the two conjugate stations indicative of a wave structure which is delayed with respect to such appearance over the equator has been verified to be a regular quiet time feature during the COPEX campaign period, and the ~40-min delay observed in this case appears to represent a typical case of SF development sequence. We should note that an echo source separated in range by 50 km from the

Table 1. Coordinates of the COPEX Stations and Those of Sao Luis and Cachoeira Paulista

	Cachimbo	Boa Vista	C. Grande	São Luís	C. Paulista
Latitude (deg)	9.5S	2.8N	20.5S	2.6S	22.7S
Longitude (deg)	54.8W	60.7W	54.7W	44.7W	45W
Dip angle	−4.2	22.0	−22.3	−3.85	−33.7
Magnetic latitude	−2	11	−11	−1.6	−16
Declination	−16.7	−14	−15.1	−20.7	−20.6

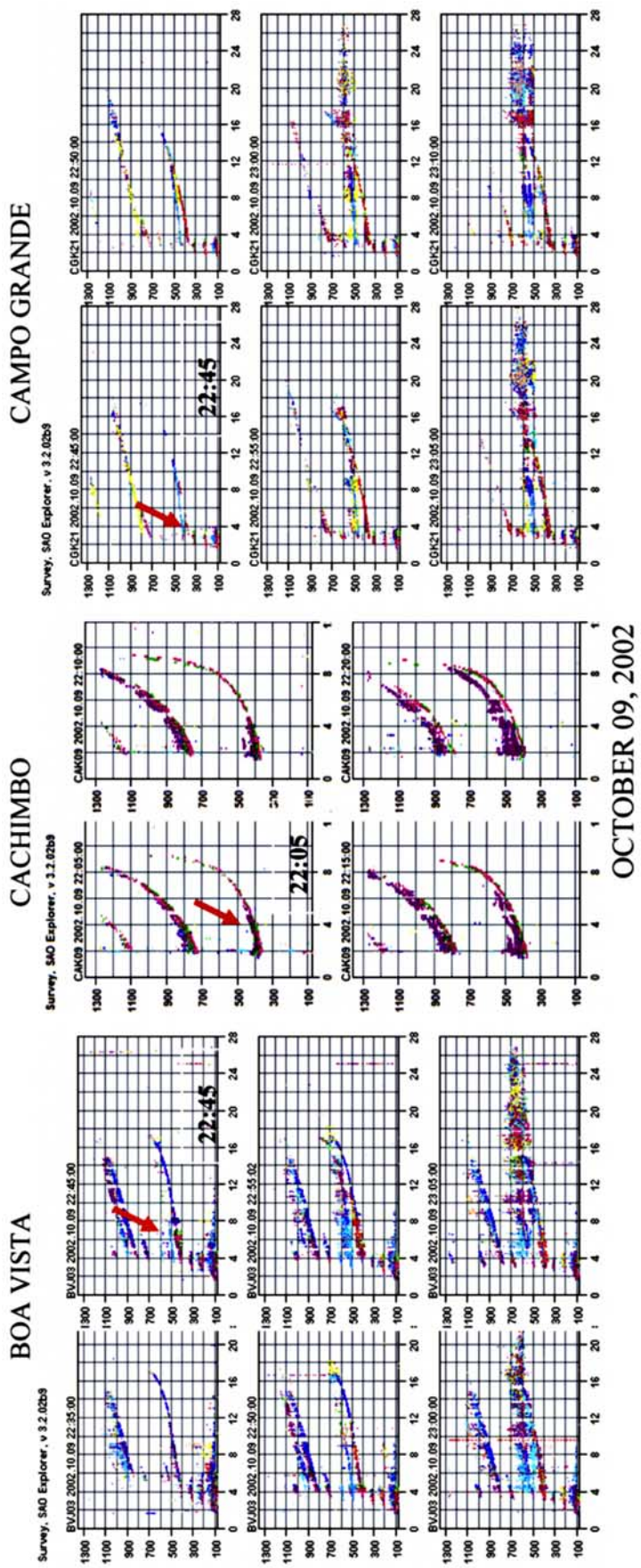

Figure 2. Sequential ionograms over (left) Boa Vista, (middle) Cachimbo, and (right) Campo Grande. The arrows pointed at the *F* layer traces at each station show the first appearance of an off-vertical trace close to the main *F* trace, indicative of the start of a large-scale "wave structure" as a precursor to the range spreading. The time delay between the first appearance of the "wave structure" at Cachimbo (at 2205 UT) and that at the two conjugate stations (at 2245 UT) indicates the vertical rise velocity (growth rate) of a flux tube–aligned bubble developing over the equator. (The additional traces that appear prior to 2245 over Boa Vista are caused by multiple reflections between the sporadic *E* layer and the *F* layer).

Table 2. Instruments Deployed in the COPEX Campaign

Site	Instrument Network
Boa Vista	Digisonde DPS4; all-sky imager; GPS scintillation monitor (2); GPS TEC monitor; VHF receivers; magnetometer
Cachimbo and Alta Floresta	Digisonde DPS4; GPS scintillation monitor (2); GPS TEC monitor; VHF receivers; 30 MHz radar
Campo Grande	Digisonde DPS4; all-sky imager; GPS scintillation monitor (2); GPS TEC monitor; VHF receivers; magnetometer
São Luís	Digisonde DGS256; GPS scintillation monitor; magnetometer
C. Paulista	Digisonde DGS256; GPS scintillation monitor

main vertical trace at 450 km (as in this example) corresponds to a horizontal separation of the reflection points by ~200 km. Observations of such oblique traces as precursors to SF have been reported before from single station observation over Fortaleza [*Abdu et al.*, 1981a] and they seem to correspond to large-scale wave structures similar to that discussed by *Tsunoda* [2008] from observations by the Altair incoherent scatter radar and ionosonde. The time delay in the appearance of the wave structures just described above has important implications on ESF development mechanism which will be discussed later.

[8] Later in the night well-developed bubble structures drifted from the west into the all-sky imager field of view over Boa Vista and Campo Grande, nearly simultaneously. Figure 3 shows two sets of airglow depletion images, one for 0300 UT/2320 LT and another for 0330 UT/2350 LT, together with the corresponding ionogram spread *F* manifestations over the two stations. These bubble structures appear to have developed westward of the COPEX station probably initiated by a vertical drift increase in the preceding hours (near 0100 UT), although the magnetic indices suggested a moderately quiet night. The imagers' field of view covers 1800 km in diameter at a reference altitude of 250 km, with maximum coverage extending to approximately ±20° of geomagnetic latitude. The higher-latitude extremities of the depletions correspond to an equatorial apex height of >1000 km. The depletions in Figure 3 thus correspond to well-developed bubble structures, and they drift eastward following their development at a westward longitude. We may note that the field-aligned airglow depletions are almost completely symmetric over the two conjugate locations. All-sky imageries from previous conjugate point observations conducted in the Asia-Oceania longitude sector by *Otsuka et al.* [2002] that used significantly larger latitudinal separation than in the present experiment showed nearly perfect symmetry of the conjugate airglow depletions. The bubble zonal drift velocities in the present experiment are also symmetric over the conjugate sites as discussed in the companion paper by *Sobral et al.* [2009]. *L* band scintillation was present over Boa Vista and Campo Grande, with S_4 index attaining ~0.8 in discontinuous patches along all the monitored GPS satellites tracks (26), but with little scintillation over Cachimbo. The brighter background intensity of the 630 nm emission in these images indicates the equatorial ionization anomaly distribution. A faint circular feature (with reduced emission intensity) appears on the right side/eastern half of the image over Boa Vista which is absent over Campo Grande. The f_oF_2 values (not shown here) are also asymmetric correspondingly.

[9] The spread *F* traces in the ionograms over Boa Vista and Campo Grande corresponding to these optical images are shown on the left side of Figure 3. The off-vertical spread *F* traces such as in the 0300 UT and 0330 UT ionograms are formed by coherent scatter returns from field-aligned irregularities inside the depletions (bubbles) [*Sales et al.*, 1996]. Their appearance for frequencies $f < f_oF_2$ indicates that the depletions extend to the bottom of the *F* layer. The spread *F* trace for $f > f_oF_2$ indicates that the F_2 depletion reaches at least up to h_mF_2, and likely into the topside. An increase in the top frequency of the spread *F* trace (often exceeding the f_oF_2) indicates a decrease in the irregularity scale sizes detected by the Digisonde. For *f* just above f_oF_2, the *F* layer trace in the Campo Grande ionogram shows a negative slope (indicated by arrow) which is caused by the group retardation decreasing with increase of frequency, owing to the underlying F_2 layer. We may note that the irregularity strength and size distributions as indicated by the SF traces appear significantly asymmetric at the two stations, being less evolved over Campo Grande as compared to Boa Vista. We consider the range of spreading (in kilometers) as a qualitative measure of the spread *F* intensity for our discussion. The top scattered frequency of the *F* layer trace, indicative of the smallest scale size of the backscattering irregularities, is also a measure of the ESF strength, which was perceivably smaller over CG than over BV conforming to the asymmetry. In view of the fact that the DPS-4 sounders and their antenna systems were identical at the conjugates stations the presented asymmetry appears to arise from a difference in the SF characteristics at the two stations. This behavior contrasts with the near total symmetry observed in the optical images of the larger-scale bubble structures [see also *Sobral et al.*, 2009]. There are many cases of such symmetry/asymmetry situations of the irregularity structures observed during the COPEX campaign. Further aspects on this question will be discussed in section 4.

3.2. Characteristics of the Evening Vertical Plasma Drift (Zonal Electric Field)

[10] Vertical plasma drift velocity was calculated from the time rate of change of the *F* layer true heights, $d(hF)/dt$, at specific plasma frequencies as obtained from the SAO software of the Digisonde system [*Reinisch*, 1996; *Khmyrov et al.*, 2008]. The velocities so obtained are comparable with the vertical velocity calculated from the drift mode operation of the DPS-4 with the utilization of the Drift Explorer software [*Abdu et al.*, 2006a; *Kozlov and Paznukhov*, 2008]. These velocities correspond to the vertical displacement of the plasma densities responsible for the radio wave reflection. It has been shown from theoretical calculations [*Bittencourt and Abdu*, 1981] and experimental validation [*Scali et al.*, 1995] that such velocities are identical to the vertical plasma drift velocities, for heights near and above 300 km where the recombination effect becomes negligible. Test was also done by comparing such velocities with the drift velocity from echo Doppler measurements obtained by the Digisonde drift explorer software [*Abdu et al.*, 2006a] and in some cases (outside the COPEX data sets) with ion

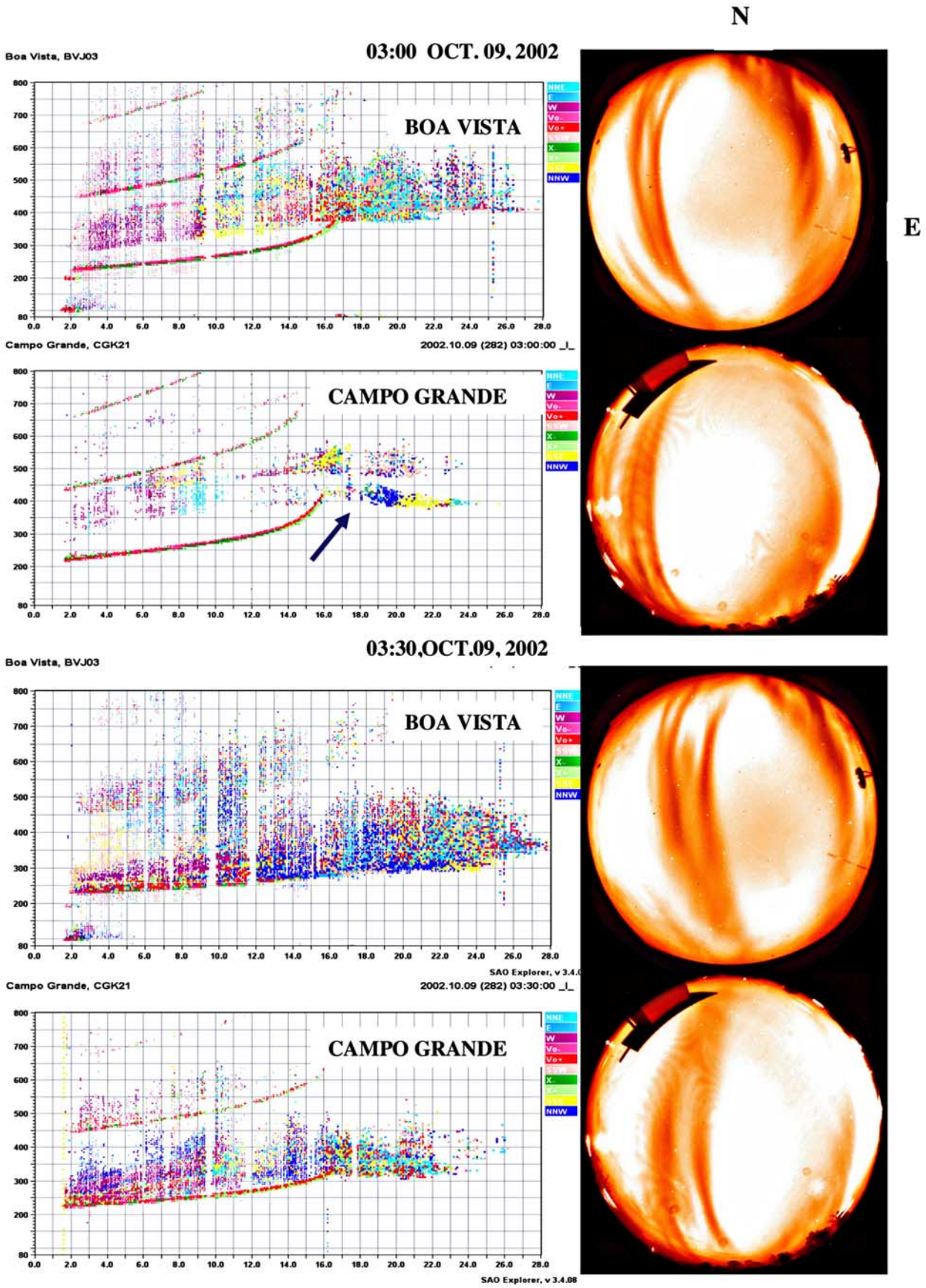

Figure 3. Illustrative ionograms over Boa Vista and Campo Grande and the simultaneous all-sky images on the night of 9 October 2002.

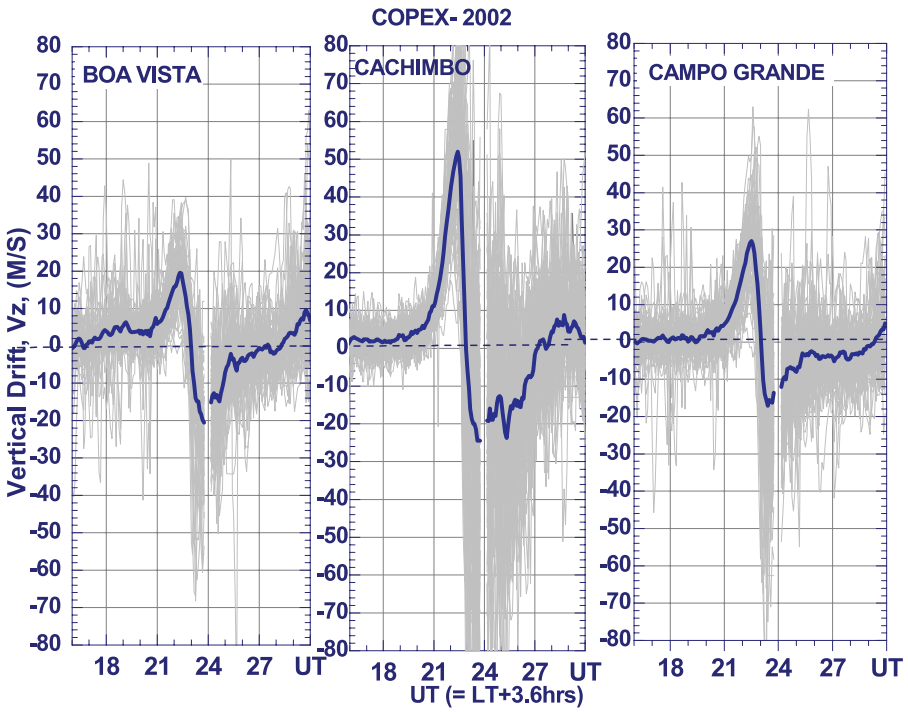

Figure 4. Vertical drift velocities versus UT over the three COPEX sites mass plotted for the entire campaign period.

drift measurements by the Jicamarca incoherent radar [*Bertoni et al.*, 2006]. Usually for plasma frequencies above 4 MHz, but not when very close to the f_oF_2, the results at different frequencies are generally comparable during evening hours when the *F* layer rises up under the prereversal enhancement in the zonal electric field. The results presented here consist of vertical drifts (V_z) measured at four plasma frequencies, 4 MHz, 5 MHz, 6 MHz, and 7 MHz. The V_z values obtained as the mean of the velocities at 4 and 5 MHz were compared with those obtained as the mean of the V_z values at 6 and 7 MHz. The two sets of the mean V_z values are found to be in general agreement. Therefore we have used both sets of V_z values in the analysis presented here.

[11] Figure 4 presents mass plots of vertical drifts over the three stations for all days of the COPEX campaign. The mean of all the V_z values are shown by the thick solid curve. Here we focus on the characteristics of the evening prereversal enhancement (PRE) in the vertical drift. The peak in the PRE has a mean value of 52 m/s over Cachimbo. Over Boa Vista and Campo Grande the velocities are significantly smaller, 20 m/s and 26 m/s, respectively. The prereversal enhancement peaks at ~1850 LT (2230 UT) at all the stations. Interesting characteristics of the PRE in these results are (1) the significant decrease of its intensity over the conjugate sites as compared to that over the equatorial site and (2) a noticeable asymmetry in the intensity at the conjugate sites. On the basis of considerations of field line mapping of large-scale electric fields the variation with latitude of the prereversal electric field as seen in this result corresponds to a height variation in the equatorial plane. Thus we note a significant decrease of the evening zonal electric field with height. The mean pattern shows a zonal electric field of ~1.2 mV/m, corresponding to a vertical drift of ~52 m/s, at a reference height of 450 km, which decreased to about half its value at ~650 km, the field line apex height for conjugate *F* layer bottomside at 350 km. (This decrease is less by 8% if we correct for the magnetic field inclination of 22° of the conjugate sites). Such negative height gradient of the evening zonal electric field has been observed by the Jicamarca radar for solar minimum flux levels [see, e.g., *Pingree and Fejer*, 1987]. For $F10.7 \approx 150$, identical to the mean flux values representing the COPEX campaign period, the available Jicamarca measurements (B. Fejer, private communication, 1990) indicates a slower decrease rate with altitude of the evening vertical drift. This would suggest the existence of a significant longitudinal variation in the vertical gradient of the evening zonal electric field between Jicamarca and the COPEX stations, which needs to be investigated further. An asymmetry in the PRE amplitude between the two conjugate sites can be noted, the amplitude over CG being larger than over BV. This would indicate the presence of an average northward transequatorial wind during the COPEX period, the details of which will be discussed later.

3.2.1. Evening Vertical Drift Enhancement and Spread *F* Development

[12] The most important prerequisite for the generation of the postsunset spread *F*/plasma bubble irregularities is the uplift of the evening *F* layer due to the prereversal enhancement in the zonal (eastward) electric field [*Farley et al.*, 1970; *Abdu et al.*, 1983b; *Fejer et al.*, 1999]. It is known that ambient conditions other than the PRE (such as those mentioned earlier) have roles to play in the control of the SF development. Below we will first examine the different aspects of the control of SF generation by the PRE. Some aspects on the evening prereversal vertical drift for spread *F* occurrence/nonoccurrence conditions over the equatorial

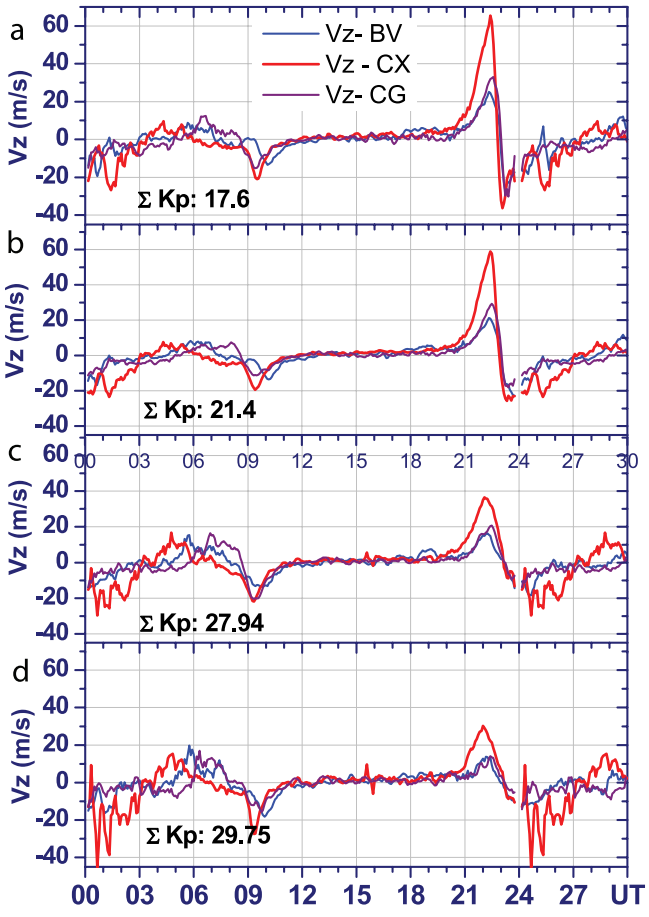

Figure 5. Mean vertical drift velocities over the three COPEX sites are plotted for different groups of days: (a) for the cases of early spread *F* occurrence (at or before 2000 LT) over Cachoeira Paulista; (b) for the group of days when SF occurred at and before 2200 LT over CP; (c) for the group of days when SF did not occur before midnight over Cachoeira Paulista; and (d) for the group of days when SF did not occur over Campo Grande and CP. (ΣKp is the daily sum of the 3-hourly *Kp* values representing its mean value for the days considered). Station names are BV, Boa Vista; CX, Cachimbo; and CG, Campo Grande. In the *x* axis the LT exceeding 24 h corresponds to a new day so that 24 should be subtracted from those values.

site, Cachimbo, have been briefly presented in a paper by *McNamara et al.* [2008] and will not be discussed here. Below we will present the results of an analysis of the vertical drift over Cachimbo as well as over the two conjugate stations as a function of the spread *F* onset/occurrence local times at the latter two stations and at a southern low-latitude site, Cachoeira Paulista (dip angle: −33.7°). Possible influences of the transequatorial winds on the ESF development will also be discussed in this and subsequent sections.

[13] Figures 5a–5d present the mean V_z values representative of the days sorted out on considerations of systematic increase in time delays for SF occurrence at latitudes farther away from the dip equator. In this context we have included also in the analysis the Cachoeira Paulista (CP) site that is not aligned in magnetic meridian with the COPEX stations, and is located at higher magnetic latitude than the southern conjugate site Campo Grande. We consider here (as also pointed out earlier) that the vertical growth of the flux tube–aligned plasma depletions over the equator, with the associated smaller-scale structures, is responsible for the latitudinal extension of the spread *F* so that its occurrence over CP (as over the conjugate sites) can be considered to indicate the bubble vertical extension to the equatorial apex height of the field line that maps to the *F* layer bottomside over these stations [see also *Abdu et al.*, 1983a]. The average ΣKp values corresponding to the sorted group of days are also shown in Figures 5a–5d. We may point out that in the evening and early night hours (and whenever the *F* layer height is >300 km, in general) the V_z values do represent realistic vertical drift. On the basis of the flux tube–aligned bubble development just stated above the spread *F* occurrence at early postsunset local times (before 2000 LT) over Cachoeira Paulista corresponds to rather fast vertical bubble rise velocities (>100 m/s) over the equator. Any effect from possible eastward drift of the bubble on the vertical velocity so estimated is expected to be small as discussed by *Abdu et al.* [1983b]. The mean V_z variations corresponding to all such cases observed during the period are plotted for the three COPEX stations in Figure 5a. The V_{zp} over Cachimbo (magnetic equator) for this case is ∼62 m/s. A second group of SF events occurring at and before 2200 LT over CP is represented by the mean V_z variations shown in Figure 5b. In this case the mean V_{zp} (over Cachimbo) is only slightly smaller, being 59 m/s. The results in Figure 5c show the case of SF not occurring till midnight over CP, which signifies that the vertical bubble growth over the equator did not attain till midnight an apex altitude of 900 km that is field line mapped to the bottomside *F* region over CP. The V_{zp} over Cachimbo for this case is around 35 m/s. The field line apex height for Campo Grande bottomside *F* region is ∼650 km. For the cases of postsunset spread *F* not occurring over Campo Grande the mean V_z variation is shown in Figure 5d. The value of V_{zp} for this case is 30 m/s which suggests that bubble vertical growth to ∼650 km could be possible when the prereversal vertical drift is higher than this value. During the campaign period there were only two non–spread *F* nights over Cachimbo (and all other stations). For those cases the mean V_{zp} (not shown here) was just 22 m/s, which can be considered to be the threshold minimum below which bottomside spread *F* did not occur over the equator. We note thus that the average V_{zp} presents a trend suggesting its systematic control on the spread *F* development, with the lowest V_{zp} (22 m/s) for the case of SF totally absent to the highest V_{zp} (∼60 m/s) for an early SF occurrence over CP corresponding to a rapid (>100 m/s) vertical growth of the bubble over the equator. We may point out that the average PRE amplitudes over the conjugate sites were significantly smaller than over the equator and their asymmetry suggested the presence of a generally weak, and northward, transequatorial wind in the *F* layer bottomside, in all the cases considered above (as in Figure 4). It is relevant to mention here that threshold conditions on the evening prereversal vertical drift for UHF and *L* band scintillation occurrence in the Peruvian sector have been discussed by *Anderson et al.* [2004]. We note further that the ΣKp values given in Figures 5a–5d present a systematic increase with decreasing evening

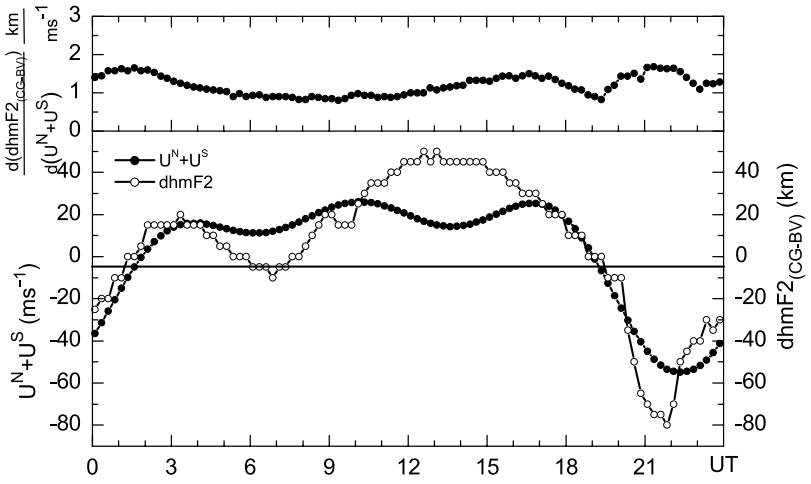

Figure 6. The bottom plot shows the SUPIM simulation results on the difference in h_mF_2 between the two conjugate stations, $\Delta h_mF_{2(\mathrm{CG-BV})}$, obtained by subtracting the h_mF_2 simulated over Boa Vista from that over Campo Grande and the corresponding transequatorial wind (TEW) (sum of the meridional winds at the two conjugate locations according to the HWM93). The top plot shows the corresponding ratio of $d(\Delta h_mF_2)/\Delta(U^{\mathrm{N}} + U^{\mathrm{S}})$.

vertical drift velocities, when at the same time the presunrise vertical drift presented a systematic increase. This point will be discussed in section 4.

3.3. Transequatorial Winds From Interhemispheric Symmetry/Asymmetry in h_mF_2

[14] In the absence of plasma transport by meridional wind and electric field the *F* layer peak electron density occurs at a height h_0 where a balance between recombination and diffusion prevails [*Rishbeth et al.*, 1978]. Depending upon the magnetic field inclination a horizontal meridional wind (as well as a zonal electric field) can cause upward or downward displacement of the *F* layer with respect to h_0 producing the observed *F* layer peak height, h_mF_2. In the presence of a transequatorial wind the h_mF_2 increases in the upwind hemisphere while it decreases in the downwind hemisphere. On the other hand any vertical displacement of the *F* layer due to large-scale zonal electric fields (such as from the *E* and *F* layer dynamo) should be equal at the conjugate locations. In this way a difference in the h_mF_2 (Δh_mF_2) observed between two magnetically conjugate locations is a good indicator of the sum of the meridional winds at the two locations. The relationship between the Δh_mF_2 from conjugate stations and transequa-

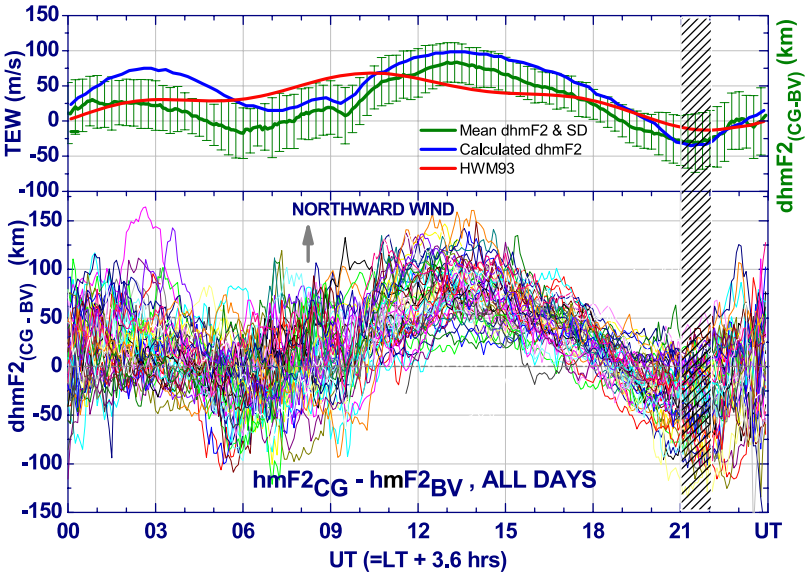

Figure 7. The bottom plot shows a mass plot of the parameter $\Delta h_mF_{2(\mathrm{CG-BV})}$ observed on all days of the COPEX campaign. In the top plot the green curve shows the mean values with standard deviation of the mass plot, the blue curve represents the $\Delta h_mF_{2(\mathrm{CG-BV})}$ modeled by the SUPIM using the meridional wind input as per the HWM93, and the orange curve shows the corresponding transequatorial wind (TEW).

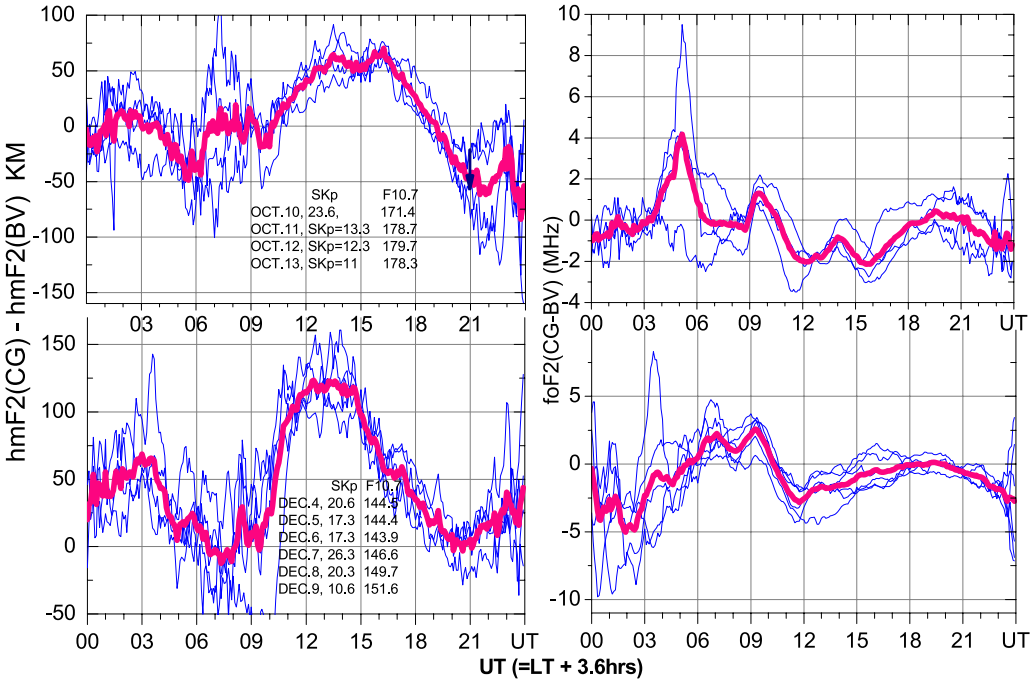

Figure 8. The $\Delta h_m F_{2(\mathrm{CG-BV})}$ parameter for (left) 4 quiet days of October and 6 quiet days of December 2002 and (right) the corresponding $\Delta f_o F_{2(\mathrm{CG-BV})}$ variations. The results for October (December) are in the top (bottom) plots.

torial winds has been studied by *Bittencourt and Sahai* [1978] using a tropical *F* region computational model. In the present investigation we have used the Sheffield University Plasmasphere-Ionosphere Model (SUPIM) code [*Bailey and Balan*, 1996] to quantify the connection between the $\Delta h_m F_2$ and the transequatorial wind for the COPEX conjugate stations as a function of UT (UT = LT + 3.6 h). A methodology to calculate the equatorial zonal electric field and low-latitude magnetic meridional winds based on $h_m F_2$ and $f_o F_2$ over equatorial and low-latitude ionosphere by the use of the SUPIM code has been discussed by *Souza et al.* [2000]. The modeling results presented in Figure 6 (bottom) show the $\Delta h_m F_{2(\mathrm{CG-BV})}$, that is, $h_m F_2$(Campo Grande) − $h_m F_2$(Boa Vista), as modeled using the SUPIM code in which the HWM93 wind [*Hedin et al.*, 1996] was one of the controlling input parameters. The zonal electric field, the other critical input parameter to the SUPIM, was based on the *Scherliess and Fejer* [1999] model that was modified by replacing the evening vertical drift with that calculated from the COPEX Digisonde data [see also *de Medeiros et al.*, 1997]. The calculation was done for conditions representative of October 2002. The sum of the meridional winds at the northern and southern conjugate stations, $U^{\mathrm{N}} + U^{\mathrm{S}}$, representative of this period, according to the HWM93 (that yielded the above $\Delta h_m F_{2(\mathrm{CG-BV})}$) is also shown in Figure 6 (bottom). Positive (negative) $\Delta h_m F_{2(\mathrm{CG-BV})}$ indicates northward (southward) transequatorial wind (TEW). The TEW is normally northward during much of the daytime and near midnight during this period (in October) in the model, which is in general agreement with the observational results presented here, in Figure 7 and in Figure 8 (to be discussed below). The model results show that a magnitude of 1 km in the $\Delta h_m F_{2(\mathrm{CG-BV})}$ corresponds on an average to a TEW of 1 m/s and their ratio does not remain constant. The ratio of a change in $\Delta h_m F_{2(\mathrm{CG-BV})}$ (in km) to a causative change in TEW (in m/s), that is, $\mathrm{d}(\Delta h_m F_{2(\mathrm{CG-BV})})/\mathrm{d}(U^{\mathrm{N}} + U^{\mathrm{S}})$ as calculated by the SUPIM for the same period is plotted in Figure 6 (top). We may note that this value varies around unity as a function time for most of the daytime with slightly higher values during night hours. This information on the coefficient, $\mathrm{d}(\Delta h_m F_2)/\mathrm{d}(U_{\mathrm{S}} + U_{\mathrm{N}})$, is useful for quantifying any conjugate point difference in $h_m F_2$ in terms of its driving transequatorial winds vis-à-vis implications on possible ESF development arising there from. (The day-to-day variations and medium-term trends in $\Delta h_m F_2$ and possible implications on SF will be discussed in section 3.5.)

[15] Figure 7 (bottom) presents a mass plot of all the observed $\Delta h_m F_{2(\mathrm{CG-BV})}$ values during the entire campaign period as a function of UT. The mean of these values with their standard deviations is shown separately (top, green curve) which presents a dominant diurnal oscillation superimposed by a less significant semidiurnal oscillation. The north direction is upward (as in Figure 6) indicated by an arrow. During most of the daytime (from ~0600 to 1600 LT) the COPEX average $\Delta h_m F_{2(\mathrm{CG-BV})}$ suggests a TEW directed northward, whereas it tends to be southward in the presunrise (near 0300 LT) and evening (around 1800 LT) hours. For this case as well the $\Delta h_m F_{2(\mathrm{CG-BV})}$ parameter was modeled by the SUPIM as an average pattern representative of the entire campaign period. The results represented by the blue curve in Figure 7 (top) show general agreement with the mean curve of the observational data. However, some disagreement is present at local times around midnight (0300 UT and around midday (1500 UT)

when the modeled $\Delta h_m F_{2(\mathrm{CG-BV})}$ are close to, or exceed, the upper limit of the SD (standard deviation) bars of observed values. The TEW according to the HWM93 that was used in the SUPIM calculation is plotted as the orange curve in Figure 7 (top). We may note that the variations in the two parameters are not in phase. In other words, the relationship between the two quantities, the TEW (according to the HWM93) and the $\Delta h_m F_2$ (that resulted from the calculation), representing the average conditions of the entire period, vary with local time in much the same way as they did in the example for October shown in Figure 6 (bottom). The extent to which the TEW requires modification to obtain a more perfect agreement between the modeled and measured $\Delta h_m F_{2(\mathrm{CG-BV})}$ will give a better idea as to how well the HWM93 represents the horizontal meridional wind pattern over Brazil during the COPEX period. Such an effort is in progress. Discrepancy between conjugate *F* layer base heights (*h'F*) as modeled by including the HWM93 and that obtained from observations has recently been reported by *Maruyama et al.* [2007] for Asian longitudes.

[16] We note large day-to-day variability in the transequatorial winds (Figure 7, bottom). Different groups of quiet days were considered separately to verify the presence of any medium-term variation in the diurnal pattern of these winds. Examples for a few quietest days of October and similar days in December are presented in Figure 8, in which both the $\Delta h_m F_{2(\mathrm{CG-BV})}$ and $\Delta f_o F_{2(\mathrm{CG-BV})}$ variations are shown. The diurnal pattern that indicates northward directed TEW (during most of the daytime and near midnight) support the model results of Figures 6 and 7. In the left plots we note that the $\Delta h_m F_2$ indicates an increasingly more northward TEW from October to December, which might be due to the increase in the solar declination angle, with the subsolar point for the thermospheric UV absorption moving well into the southern hemisphere toward the later part of the COPEX campaign period. The predominantly northward winds seem to be responsible for a significant decrease in the $h_m F_2$ over BV for most of the time as verified from the data (not shown here). The corresponding $\Delta f_o F_{2(\mathrm{CG-BV})}$ plots in (Figure 8, right) highlight, as the main point, a generally negative $\Delta f_o F_2$ which intensifies during most of the night hours in December, which is a reflection of an increase of $f_o F_2$ over Boa Vista at those hours (not shown here). This result suggests that a northward wind over Boa Vista in the night, which in this case is part of a transequatorial system, brings plasma down along the field lines, (apparently at a rate faster than the recombination rate), contributing to the increase of the $f_o F_2$ over this station. On the other hand, during daytime we see a different picture. In December, when the transequatorial wind is more intense than in October, the $\Delta f_o F_{2(\mathrm{CG-BV})}$ did not show any correspondingly significant increase, which may be attributed to the influences from daytime dynamical/electrodynamical and photochemical processes. In fact the daytime $f_o F_2$ values at both stations (not shown here) were less in December than in October, which would suggest that the equatorial anomaly fountain might be somewhat weaker during these December days than it was in October. This fact, even in the presence of an asymmetric ion production rates at the conjugate sites with the CG being much closer to the sub solar point than BV in December, appears to have contributed to a reduction of the $\Delta f_o F_{2(\mathrm{CG-BV})}$ values in December as compared to October in Figure 8. Further analysis of this problem could lead to a better understanding of the seasonal features in the equatorial fountain/anomaly vis-à-vis the possible role of transequatorial winds in such features.

3.4. Transequatorial Winds and ESF

[17] We may note that the larger southward TEW (represented by the larger negative $\Delta h_m F_2$) that dominated the evening hours of the October quiet days was almost totally absent during the December interval (Figure 8). A potential effect on ESF generation arising from such a change in the evening wind direction is an interesting possibility that needs to be investigated (see section 4). A transequatorial wind, whether directed northward or southward has the potential to suppress the postsunset ESF [e.g., *Maruyama*, 1988; *Abdu*, 1997; *Abdu et al.*, 2006b]. This point can be addressed in terms of statistical as well as on a case study basis. We will here examine some specific cases in the COPEX data set which seem to provide evidence of ESF suppression by the transequatorial wind. In the example in Figure 9a we present the evening vertical drift (due to the PRE) over Cachimbo, Boa Vista, and Campo Grande. The three days of 10, 12 and 23 October, when the V_z variations during the PRE are very much identical over Cachimbo, are plotted in the Figure 9a (left). The corresponding V_z variations over the conjugate stations (Figure 9a, middle and right) show significantly reduced V_z amplitude like in the statistical plot of Figure 4. On two days, i.e., 10 and 12 October, the evening V_z variations are nearly identical/symmetrical and are relatively larger (35 m/s) than on 23 October at the two conjugate stations. The symmetry would indicate the presence of nearly zero transequatorial wind at these hours. Correspondingly the vertical development of plasma bubbles is indicated in the sequence of ionograms over Campo Grande (mag. lat.:12°S) starting at 2250 UT on 10 October (Figure 9b). The oblique trace starting at 2250 UT developing into spread *F* traces in successive ionograms is a clear indicator of bubble development, as the trace first appeared over CX at 2210 UT (not shown here) followed by near simultaneous appearance, after a time delay of ~40 min, over the two conjugate sites. This time delay (40 min) in the SF onsets over the conjugate sites, relative to that over the equator, points to a bubble vertical rise/development velocity of ~125 m/s (based on consideration of the conjugate point bottomside *F* layer at ~350 km being field line mapped to equatorial apex height of ~650 km). An exactly similar description holds for the spread *F* development sequence over the three stations on 12 October (also not shown here to save space) which was also marked by V_z variations identical to that of 10 October. On the other hand, the V_z variation on 23 October (day 296) shows asymmetric patterns at the two conjugate stations, the peak amplitude of V_z (V_{zp}), at Campo Grande being 8 m/s larger than at Boa Vista. This might correspond to a northward (transequatorial) wind of ~25 m/s. The exact relationship between the ΔV_{zp} and TEW will be shown later. The *F* layer traces at Campo Grande for this evening, presented in the bottom half of Figure 9b, do not show any overhead spread *F* thereby suggesting total absence of any field-aligned topside bubble development in the COPEX station meridian (even though the vertical drift of 75 m/s

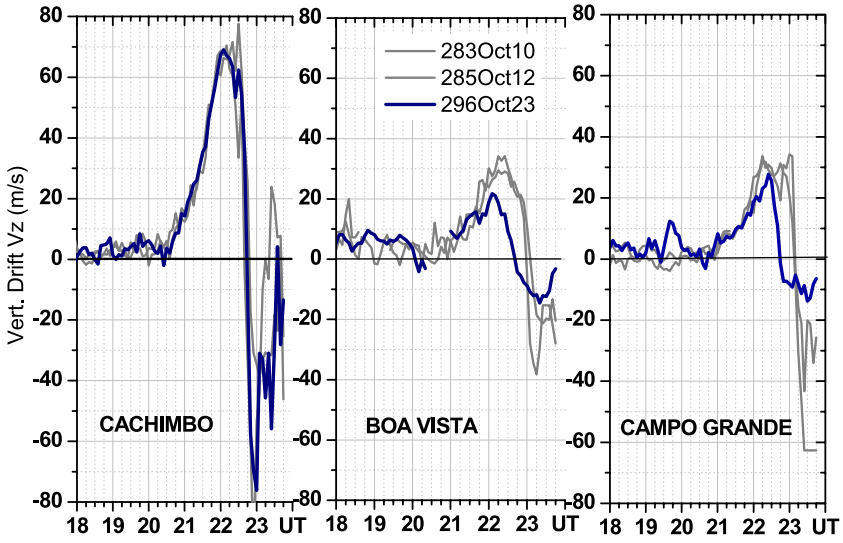

Figure 9a. Vertical drift velocities over (left) Cachimbo, (middle) Boa Vista, and (right) Campo Grande during 3 quiet days, 10, 12, and 23 October. They were nearly equal on all 3 days during sunset time over Cachimbo, on 2 days (10 and 12 October) they were comparable/symmetric, and on 1 day (23 October) they were asymmetric over the conjugate stations.

over the equator was well above the threshold limit for the bubble development, under very weak TEW, as discussed in section 3.2.1). This sequence appears to provide direct evidence on the postsunset ESF suppression by the transequatorial wind. It is a significant result from the COPEX campaign that is also supported by our recent findings on ESF suppression by meridional winds as obtained from Digisonde data analysis, but using a different methodology [*Abdu et al.*, 2006b].

3.5. Medium-Term Trend in the Transequatorial Wind and Evening Vertical Drift

[18] The evening vertical drift peak (V_{zp}) values at Cachimbo, obtained from the mean of the vertical drift variations calculated using two pairs of frequencies (4 and 5 MHz and 6 and 7 MHz), are plotted in Figure 10a as a time series during the entire COPEX campaign period. It is to be noted that the V_{zp} values derived from the two frequency pairs are in general comparable to each other (with a few exceptions). The solar flux parameter $F10.7$ is plotted in Figure 10b. The difference between the V_{zp} values at the conjugate sites, $V_{zp}(CG) - V_{zp}(BV)$, denoted as $\Delta V_{zp}(CG - BV)$, is plotted in Figure 10c. The difference between the conjugate point h_mF_2 values, as an average of the 5-min values in the 1800–1900 LT interval (indicated by shaded area of Figure 7), denoted as $\Delta h_mF_2(CG - BV)$, is plotted in Figure 10d. We note large day-to-day variability in the V_{zp}, ΔV_{zp} and Δh_mF_2 values. Notwithstanding the same, the V_{zp} values show an increasing trend, as seen in the linear fit (Figure 10a), its average value increasing by ~10 m/s from early October to early December. Such an increase appears to be part of the seasonal variation in the V_{zp} whereby the December–January period has an annual peak in V_{zp}. Such an annual peak has been shown to be arising from the large westward magnetic declination angle that characterizes the Brazilian longitude sector [*Abdu et al.*, 1981b]. The V_{zp} is found to be strongly modulated by the $F10.7$, which brings out the well-known solar flux dependence of this parameter [*Fejer et al.*, 1991]. The large day-to-day variation in the V_{zp} during the interval from approximately the day 300 to the day 320 has been shown to be the result of a planetary wave episode [*Abdu et al.*, 2006c]. The difference between the vertical drifts at conjugate points, $\Delta V_{zp}(CG - BV)$, shows a steady increase toward December superposed on its day-to-day variability. The average values of approximately −10 m/s in early October increased to 12 m/s in early December. This steady increase in $\Delta V_{zp}(CG - BV)$ indicates a corresponding increase of northward transequatorial wind (TEW) consistent with the Δh_mF_2 variation in Figure 10d as well as with the variation from October to December for 1800–1900 LT period seen in the plot in Figure 8.

[19] The relationship between the vertical drift and meridional wind at the conjugate stations can be expressed as follows. Besides the $\mathbf{E} \times \mathbf{B}$ vertical drift arising from a zonal electric field, a meridional wind causes vertical displacement of plasma due to finite magnetic field inclination, so that the net vertical drift v_{eff} at a location with magnetic inclination I is the sum of the vertical drift due to the electric field, $v_z \cos(I)$, and that due to the magnetic

Figure 9b. The set of nine plots in the top half shows ionograms over Campo Grande at the 5-min interval from 2235 UT (~1900 LT) till 2315 UT (~1940 LT) on 10 October 2002. Development of rather intense spread *F* can be seen being initiated from the "off-vertical trace" in the 2250 UT (1910 LT) ionogram. Well-developed spread *F* traces continued past the last ionogram presented here. The bottom set of nine plots shows ionograms similar to above starting at 2310 UT (1930 LT) for 23 October 2002. Here no overhead spread *F* development is noted.

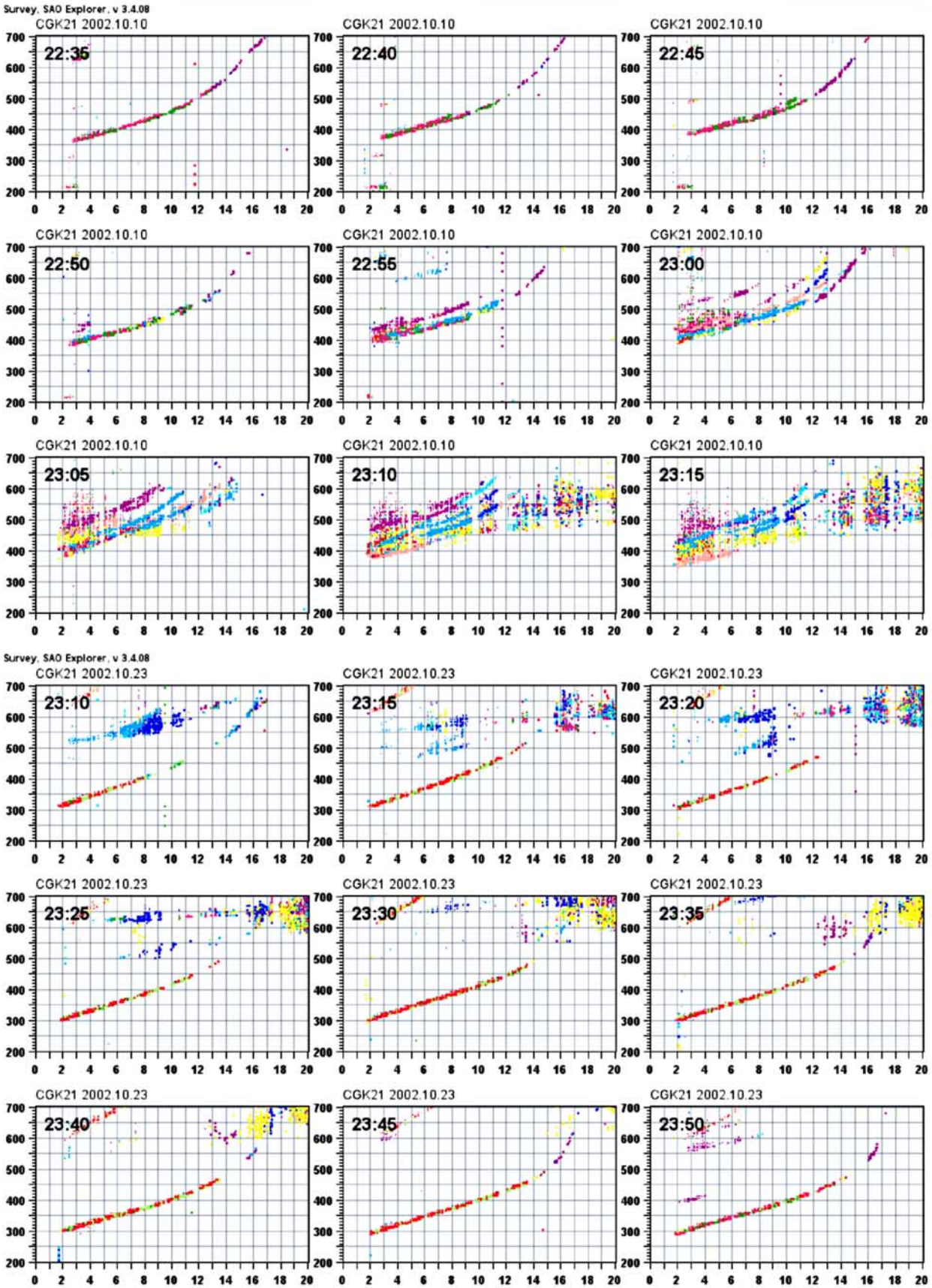
Survey, SAO Explorer, v 3.4.08
CGK21 2002.10.10
22:35
22:40
22:45
22:50
22:55
23:00
23:05
23:10
23:15
Survey, SAO Explorer, v 3.4.08
CGK21 2002.10.23
23:10
23:15
23:20
23:25
23:30
23:35
23:40
23:45
23:50

Figure 9b

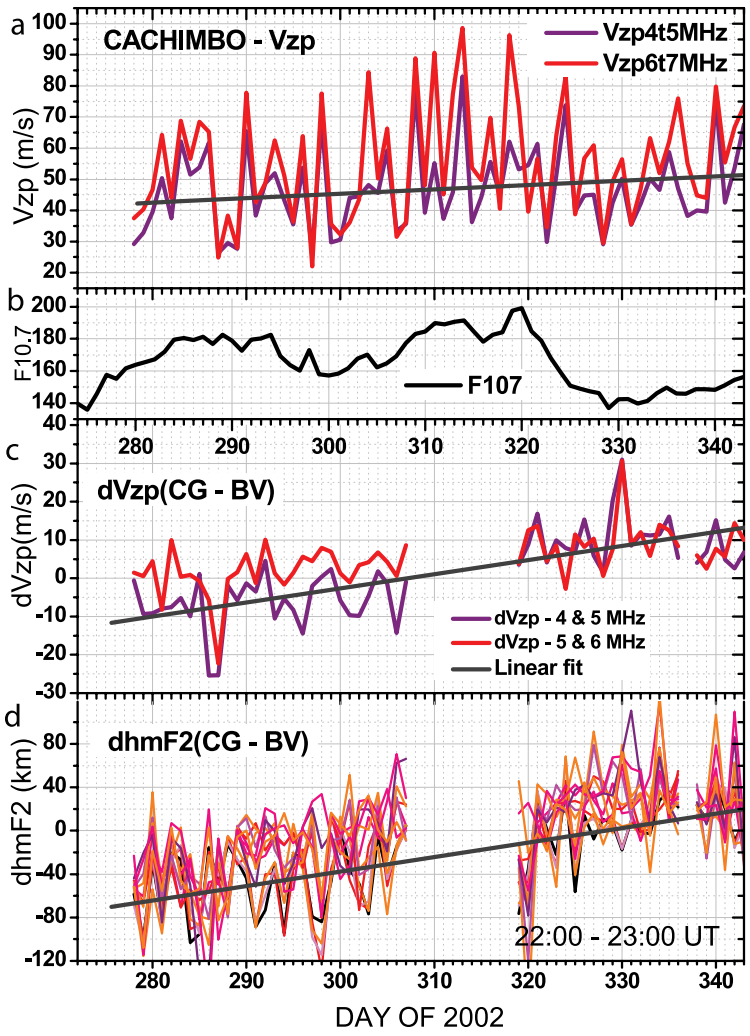

Figure 10. (a) The peak amplitude of the evening vertical drift (V_z) enhancement, V_{zp}, plotted for the entire COPEX Campaign period. (b) Solar flux index $F10.7$. (c) The difference in the V_{zp} values at the conjugate stations by subtracting the V_{zp} over Boa Vista from that of Campo Grande denoted as $dV_{zp(CG-BV)}$. (d) The corresponding difference in the h_mF_2 values denoted as $dh_mF_{2(CG-BV)}$. The data gap around day 310 is due to the fact that the BV Digisonde did not operate during this period.

meridional wind $U_{mm}\cos(I)\sin(I)$. Therefore the parameter ΔV_{zp} can be expressed as

$$\Delta V_{zp(CG-BV)} = \upsilon_{eff(CG)} - \upsilon_{eff(BV)} = (U_{mmCG} + U_{mmBV})\cos(I)\sin(I) \quad (1)$$

U_{mm} is considered positive northward in equation (1). For the dip angle of the conjugate stations (23°) a change in $\Delta V_{zp(CG-BV)}$ by 1 m/s corresponds to a change in the transequatorial wind by ~3 m/s. Thus we note (from Figure 10c) that the dV_{zp} was −10 m/s (as per the linear fit curve) during early October which corresponded a southward directed TEW of 30 m/s. The TEW became ~40 m/s northward during December (that represented an overall northward increase by 70 m/s). The average value of the coefficient $d(\Delta h_mF_2)/\Delta(U^N + U^S)$ during 1800–1900 LT, for which $\Delta h_mF_{2(CG-BV)}$ parameter is plotted in Figure 10d, is close to 1.5, in units of km/(m/s) (see Figure 6). The increase in the Δh_mF_2 from October to December in Figure 10d is found to be ~90 km, which therefore corresponds to a change in the magnitude of TEW by ~60 m/s. (possible effect of such medium-term variation in TEW on ESF will be briefly discussed in section 4). Thus we note that the change in the TEW as obtained from the V_{zp} measurement (70 m/s) is a bit higher than that inferred from the modeled h_mF_2 values (~60 m/s). Such a difference appears to be reasonable considering the rather rapid variation in the coefficient $d(\Delta h_mF_2)/\Delta(U^N + U^S)$ present around this local time (as per Figure 6) and the height difference between h_mF_2 and the F layer bottomside heights at 4–7 MHz plasma frequencies used for V_z calculation. Also, during the period (around the day 310) when ΔV_{zp} is around zero the mean (best fit) Δh_mF_2 does not become zero, presenting an offset by ~30 km. This situation seems to suggest the presence of certain hemispheric asymmetry between the COPEX stations arising from factors other than the TEW. A possible asymmetry of the neutral atmosphere, and the incident solar ionizing radiation, over the conjugate sites arising from the latitudinal separation

between the geographic and dip equators (the geographic latitude of the BV and CG being 2.8°N and 20.5°S, respectively) can be a likely cause. A quantitative verification of this point is beyond the scope of this paper. We should point out, however, that in view of the offset just mentioned above, during the hours when V_z measurement by Digisonde is reliable, particularly in the evening hours (near 1800–1900 LT), the TEW appears to be better represented by ΔV_{zp} than by $\Delta h_m F_2$ values.

4. Discussion

[20] The COPEX campaign results have brought to light some new findings/evidence on the postsunset spread *F*/plasma bubble irregularity development conditions and related issues as highlighted below. They range from the instability initiation characteristics, bubble development under the influences of the evening vertical drift (prereversal electric field enhancement), to the role of transequatorial/meridional winds on a day-to-day and medium-term basis. The results also have provided new evidence on possible control (or lack of control) of the ESF development by changes in field line integrated conductivity represented by the variable presence of sporadic *E* layers at the feet of the unstable field lines, which is the subject of a separate paper by *Batista et al.* [2008]. According to the theory of the Rayleigh-Taylor instability mechanism, believed to be responsible for the ESF/bubble development, an electron density perturbation needs to be initiated at the bottomside gradient region of a rising *F* layer for the instability to develop. The basic source of the initial perturbation, widely attributed to gravity wave flux originating from the lower atmosphere, is little understood and will not be discussed here any further. The linear growth rate for the instability process is dependent on the flux tube–integrated quantities as explained by *Haerendel et al.* [1992]. A generalized form of the linear growth rate as derived by *Sultan* [1996] is given by

$$\gamma_{FT} = \frac{\sum_P^F}{\sum_P^E + \sum_P^F}\left(\frac{E}{B} - U_{FT}^P + \frac{g}{\nu_{eff}}\right)\frac{1}{L_{FT}} - \beta_{FT} \qquad (2)$$

Here Σ_P^E and Σ_P^E are the field line integrated conductivities for the *E* and *F* region segments of a field line; U_{FT}^P is the conductivity-weighted flux tube–integrated vertical wind; β is the recombination loss rate; and ν_{eff} is the effective ion-neutral collision frequency. The subscript *FT* in equation (2) stands for flux tube–integrated quantity. The influence of the different terms in the ESF variability has been discussed briefly by *Sultan* [1996] [see also *Abdu*, 2001]. Perhaps, the most observed effect on the ESF development is caused by the *E/B* term arising from the evening vertical drift enhancement (PRE) of which new results were presented above, and will be further discussed below. We note from equation (2), that a larger flux tube–integrated conductivity could reduce the instability linear growth rate. Even if γ_{FT} is sufficiently positive for the initiation of the instability the ensuing nonlinear growth of the instability developing into topside bubble structures can be retarded or even totally inhibited depending upon the magnitude of the flux tube–integrated conductivity which can be controlled by TEW/meridional winds as discussed by *Maruyama* [1988] and observationally verified by *Abdu* [1997] and *Abdu et al.* [2006b].

[21] The ESF initiation process as detected from the appearance of the off-vertical echoes/satellite traces in the ionograms presented in Figure 2, indicates the presence of wave disturbances as precursor to the SF traces in ionograms, as was discussed by *Abdu et al.* [1981a] from ionosonde observation over Fortaleza. The result presented here from the combined observations over the conjugate and dip equatorial sites of the precursor traces has important significance for elucidating the ESF onset processes. These traces appear to represent the large-scale wave structure (LSWS) in the bottomside *F* region observed by the ALTAIR incoherent scatter radar that is identified as satellites traces in ionograms, as recently discussed by *Tsunoda* [2008]. On the basis of the diagnostics by radar and Digisonde pointing to similar feature as an ESF precursor signature we may call this off-vertical trace as LSWS trace or simply WS (Wave Structure) trace. The main *F* layer trace echoes are reflected close to vertical as verified from the second hop distance in the ionogram, and from Digisonde sky maps. The wave structure traces just mentioned usually appear from the immediate west or east of the vertical in the majority of cases. Depending upon the observational cadence (5 min in this case) the smallest detectable separation between the main trace and the closest WS trace can vary from less than 100 km to several hundred kilometers, compatible with the ~200 km east-west scale size for LSWS revealed in the steering mode incoherent scatter radar map of *Tsunoda* [2008] and the ray tracing results by *Sales et al.* [1996]. The most important aspect of the present data is the simultaneous observation of the wave structure traces in the conjugate station ionograms, whereby a new insight into the dynamics of the trace evolution emerges as described below. In nearly all the cases examined in the COPEX campaign data set, the WS traces appear nearly simultaneously at the conjugate stations. But they are delayed by a few tens of minutes with respect to their appearance over the equatorial site. Such time delay is found to vary, from one day to another, from approximately 20 min to 45 min in the cases examined under quiet conditions. If the wave structure is the signature of electron density modulation by a propagating neutral wave disturbance (such as a gravity wave) then these results, (showing simultaneous occurrence at conjugate stations that is delayed with respect to the occurrence over the equatorial station), would point (on the basis of the COPEX station alignment shown in Figure 1b) to a magnetically westward propagating neutral disturbance front in the evening hours. While westward propagating gravity waves are expected to be present in the *F* layer bottomside [*Fritts et al.*, 2008] that possibility appears unlikely to explain the present scenario given the well-known day-to-day variability of the neutral wave dynamics. On the other hand we expect the plasma bubble development by the R-T instability mechanism to take place in unstable plasma flux tubes under conditions determined by the electric fields, conductivity and perpendicular and parallel currents of the entire flux tube [see, e.g., *Haerendel et al.*, 1992; *Sultan*, 1996; *Keskinen et al.*, 2003], a situation that results in simultaneous instability growth along the entire flux tube which is manifested as vertical

development of the depleted flux tubes above the equator. The corresponding latitudinal extension/expansion of the bubble "feet" could explain the near simultaneous appearances of the WS traces over the conjugate sites that are delayed by several minutes with respect to the first appearance of such traces over an equatorial site. A time delay of 30 min for the WS appearance over the conjugate stations implies a bubble vertical rise velocity of ~120 m/s. This velocity is compatible with the available model and observational results [e.g., *Zalesak et al.*, 1982; *Tsunoda*, 1981; *Abdu et al.*, 1983a]. We note that the smaller-scale structuring manifested in the diffuse echoes of the range spread trace, as part of the bubble, is already well developed at the equator by the time the WS trace marking the bubbles initiation first appears over the conjugate locations. The observed variable time delay on different days would indicate a correspondingly variable vertical rise velocity of plasma bubble structures developing over the equator. Thus the signatures of the LSWS/WS over the equatorial and conjugates sites, as described here, can be seen as direct manifestation of the vertical development of the flux tube–aligned bubbles. Their continuing altitudinal/latitudinal development to topside bubbles structures are controlled by conditions set by the PRE, seed perturbation intensity, the transequatorial winds and the field line integrated conductivity. The present results in fact are evidence that the wave structure, manifested as off-vertical echoes, or satellite traces, in the postsunset equatorial ionograms, do indeed mark the onset of plasma bubble development. This evidence thus supports the view that the direct precursor to the ESF/plasma bubble development in the form of the LSWS seen by radar, as described by *Tsunoda* [2008], is the same as the off-vertical/satellites traces in ionogram simultaneously observed at conjugate sites as presented here as well as that reported earlier from single station observations [*Abdu et al.*, 1981a].

[22] The results in Figure 5 illustrate the control by V_z over the equator for different degrees of bubble development/rise velocity as manifested by the varying time delay in the spread *F* onset at off-equatorial latitudes. The larger evening vertical drift with peak value (V_{zp}) of around 60 m/s could result in rapid bubble rise velocity (>100 m/s) that caused postsunset spread *F* over Cachoeira Paulista at earlier postsunset local times (before 2000 LT and 2200 LT in the two cases considered). These cases can be classified as well-developed bubble events with the equatorial apex heights probably exceeding ~1000 km. Apparently the TEW that was present during these events, as indicated by a small degree of conjugate point asymmetry in the evening V_z (clearly seen in the V_{zp} values at BV and CG in Figures 5a and 5b) did not have much influence on the bubble growth in the presence of such large vertical drift. The case of the less developed bubbles with equatorial apex height not attaining the ~900 km height limit necessary for SF occurrence at Cachoeira Paulista corresponded to V_{zp} of only ~35 m/s (Figure 5c). The limit of V_{zp} for the case of the bubble growth not attaining an apex height of ~650 km, which is the limit for observing SF over the conjugate stations, is only ~30 m/s (Figure 5d). In other words, the V_{zp} should be >30 m/s for the bubbles extending to 650 km that is the minimum height necessary for spread *F* to be observable over the conjugate stations. The lowest vertical drift of 22 m/s corresponded to the case of a stable postsunset equatorial *F* region. Thus we have evidence of a systematic control by the evening vertical drift on the growth rate for the spread *F*/plasma bubble development. We note further that statistically this systematic control is not likely affected by the TEW whose magnitude, it appears, was not expressive enough in the presence of the relatively larger V_{zp} values (Figure 5). These results are in reasonably good general agreement with the results from previous studies connecting V_{zp} with the ESF intensity [e.g., *Abdu et al.*, 1983b; *Fejer et al.*, 1999] though these earlier studies did not consider the presence of the TEW. Thus, in the sense that a verification on the possible role of TEW was possible (although with little effect during the period analyzed), the COPEX data has permitted additional refinement in the relationship between the V_{zp} and ESF development. It should be pointed out here, that the picture described above is the results of a mean behavior. The connection between the changes in individual V_{zp} and ESF intensity is bound to present a good degree of variability on a day-to-day basis owing to other factors such as the amplitude of a possible seeding source, the nature of the LSWS as observed here and as considered by *Tsunoda* [2008], the presence of a TEW of larger intensity, etc.

[23] It is interesting to note in Figure 5 that the systematic decrease of the V_{zp} with the increasing delay for spread *F* onset at an off-equatorial latitude (that is, with a decrease of the bubble rise velocity) is apparently associated with a systematic increase of the ΣKp values. This might suggest that the postsunset decrease of the V_z could have a significant contribution from disturbance dynamo electric field that has westward polarity at these hours [see, e.g., *Richmond et al.*, 2003]. We may note further that the presunrise V_z, on the other hand, presents a systematic increase with the increase of the ΣKp, again an indication of the presence of disturbance dynamo electric field which is eastward during these hours. Presunrise/postmidnight increases in the *F* layer height and vertical drift near the equator occurring under quiet as well as disturbed conditions have been discussed before [*Abdu et al.*, 1996; *Nicolls et al.*, 2006]. It is interesting to note that the intensity of the TEW (as reckoned from the difference of V_z between the conjugate stations, plotted in blue and red curves in Figure 5) also increases during presunrise hours with increase of *Kp*. This might indicate the possibility of an asymmetric energy input for high-latitude thermospheric heating that drives the equatorward winds, which has, under reduced plasma density (and hence reduced ion drag effect) of the presunrise hours, easier access to equatorial latitude. The corresponding signature on presunrise ESF development needs to be examined (however, see also *MacDougall et al.* [1998]). More detailed results on the disturbance features in the COPEX results will be the topic of a different paper.

[24] The well-developed large-scale bubble structures in Figure 3 (as seen in the optical images) appear symmetrical over the conjugate stations, with their zonal drift velocities being exactly identical as well, as shown in the companion paper by *Sobral et al.* [2009]. On the other hand, the smaller-scale structures as observed in the ionograms present significant asymmetry. The background *F* layer characteristics over Boa Vista and Campo Grande were somewhat

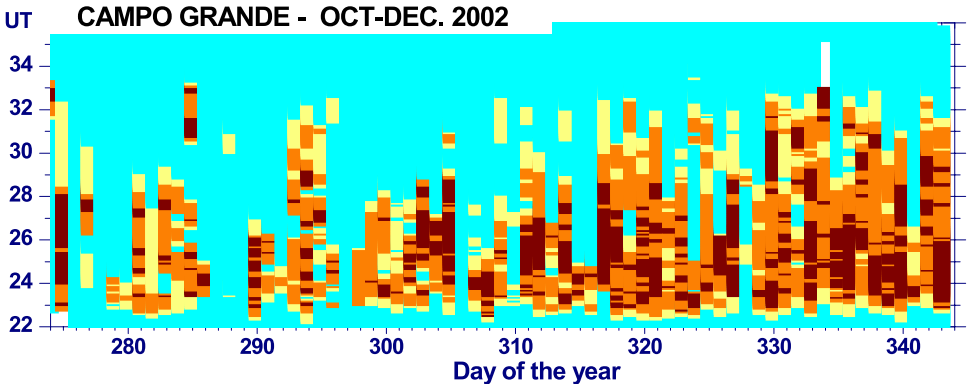

Figure 11. Ionogram spread *F* intensity, indexed as "1" (spread range <100 km, marked yellow), "2" (100 km < spread range < 200 km, marked orange), and "3" (200 km < range spreading < 300 km, marked brown), and darker shading for spread range >300 km, as a function of UT and the day of year during the COPEX campaign period.

similar but not exactly identical. We note the f_oF_2 values of 17 MHz and 16 MHz over BV and CG, respectively, which could indicate the presence of some degree of TEW directed northward at this time and hence possibly a corresponding asymmetry in the density gradient regions of the plasma bubble at conjugate locations. Results of three-dimensional simulation of plasma bubble by *Keskinen et al.* [2003] showed larger density gradients inside a bubble when the ambient density is higher. Accordingly the different ambient densities at the conjugate sites verified in the ionograms of Figure 3 could correspond to different degrees of density gradient within the bubbles and hence in the generation of secondary instabilities producing the medium-scale structures (km or smaller scale sizes) detected with asymmetric echo intensities by the conjugate site Digisondes. Also, the electric fields at such scale sizes do not field line map between the conjugate ionospheres [see, e.g., *Farley*, 1960]. This would lead us to conclude that the larger-scale plasma bubble structures are symmetric with respect to the dip equator, while the smaller scales that cause radio wave scintillations and/or spread *F* traces in the ionograms may not show hemispheric symmetry, being influenced significantly by the local ionospheric conditions. In this context it is pertinent to recall that the *L* band scintillation (measured by the GPS receivers) presented higher intensity over the conjugate sites as compared to the very weak intensity over the equator (section 3.1). The background plasma density over the conjugate sites is higher than over the equator, which could lead to density gradients in the instability development process that are more intense over the conjugate sites than over the equator (as per the modeling results of *Keskinen et al.* [2003]). Such a scenario should be an important cause of the observed scintillation intensity latitude distribution. This point deserves further investigation, however.

[25] An important feature of the evening vertical drift enhancement (prereversal enhancement in the zonal electric field (PRE)) revealed from the COPEX campaign results concerns the strong latitude/height gradient in this parameter. It appears to be more intense in the Brazilian longitude than that expected over Jicamarca for identical solar flux conditions. One of the driving factors of the PRE is known to be the thermospheric zonal wind [*Rishbeth*, 1971; *Heelis et al.*, 1974; see also *Batista et al.*, 1986] which is eastward in the evening and postsunset hours. A latitudinal variation in the evening zonal wind should be able to produce a corresponding variation in the zonal electric field as well, as it appears to do in the vertical electric field [see, e.g., *Anderson and Mendillo*, 1983]. If so, the rapid decrease of the vertical drift with increasing height/latitude might signify a correspondingly rapid latitudinal decrease in the zonal wind. This point needs to be verified from direct observations of the winds at these latitudes and from model simulation of PRE development based on such winds. The presence of a latitudinal gradient in the plasma bubbles zonal drift velocity suggesting a corresponding gradient in zonal winds in the Brazilian region has been reported by *Sobral and Abdu* [1990].

[26] One of the interesting results from the COPEX campaign concerns the features of the TEW characterized by its large day-to-day variability (Figure 7) as well as by its medium-term trend of increasing northward intensity (Figure 10). While the latter characteristics appear to originate from the solar declination angle variation during the campaign period, its possible influence on the seasonal variation of the ESF is of specific interest. The evening (1800–1900 LT) TEW varied from ~35 m/s southward in the beginning of October to as much northward in the beginning of December as per the ΔV_{zp} parameter in Figure 10c. During this period the spread *F* occurrence shows a systematic increase as part of its seasonal variation in the Brazilian longitude sector [*Abdu et al.*, 1981b; *Sobral et al.*, 2002] as shown in Figure 11 for Campo Grande. This SF seasonal trend does not clearly indicate a direct influence on its development from the TEW which should have manifested itself by a general increase of SF around the period of zero TEW. On the other hand we note that the V_{zp} variation over Cachimbo in Figure 10a (as seen in the linear fit curve) shows an increase by ~10 m/s during the same period. On the basis of the earlier discussion related to the results in Figure 5 we expect to see an increasing trend in SF occurrence/intensity as a result of an increasing trend in V_{zp}, which is indeed observed. Thus we note that the degree of medium-term variation in TEW appears to be inadequate

to dominate over the effect of a medium-term variation in V_{zp} in controlling the ESF variation trend during this campaign period that covered only a limited part of spread *F* occurrence season over Brazil. This however, may not rule out any possible role of a larger intensity variation in TEW to explain the spread *F* seasonal variation as discussed, for example, by *Maruyama and Matuura* [1984].

[27] Under unique conditions such as those represented in the results of Figures 9a and 9b it appears possible to clearly identify the role of TEW in specific cases of ESF suppression. Here, on two of the three carefully selected evenings (10 and 12 October) the vertical drifts over Cachimbo are nearly the same as are the drifts over the two conjugate stations, which indicated near-zero TEW on these evenings. Consequently bubble development was initiated at 2250 UT (1910 LT) followed by continuing evolution of the SF traces in the subsequent ionograms. In contrast to this, on the third day (23 October), while the drift over Cachimbo is almost the same as on the other two days, that over the two conjugate stations differed significantly, which corresponded to a northward TEW of ~25 m/s. On this evening overhead bubble development did not take place over the COPEX stations, which revealed only some eastward drifting patches detected later on. Spread *F* was present over Cachimbo on this evening but apparently did not develop vertically to be observed at the conjugate sites. Thus in a case study like this it looks possible to verify the effect of TEW in suppressing/limiting the growth of top side bubble development. Similar case studies demonstrating the role of TEW in suppressing the ESF were made recently by *Abdu et al.* [2006b]. In an earlier study [*Abdu*, 1997] it was pointed out that while the TEW is effective in suppressing the topside bubble development it appeared not as effective to suppress the *F* layer bottomside irregularities.

5. Conclusions

[28] The results from the analysis of the COPEX campaign data presented here have brought out new insight into the dynamical and electro dynamical processes that control the postsunset equatorial spread *F* development and evolution, besides providing new evidence in support of some of the already known aspects of the related coupling processes. The main conclusions of this study can be summarized as follows.

[29] 1. Simultaneous measurements by Digisondes at the magnetic equator and conjugate locations have enabled the identification of large-scale wave structures over the equator, that are precursor to spread *F* development, as indicating the initiation of the flux tube–aligned plasma bubbles development over the equator. This is the first evidence that the wave structures (WS) manifested as off-vertical trace in the postsunset equatorial ionograms do indeed mark the initiation of plasma bubble development. The inferred bubble rise velocities are compatible with those determined from observations and model studies.

[30] 2. While the larger-scale plasma bubbles structures as seen in optical images are fairly symmetric with respect to the dip equator the smaller scales responsible for producing spread *F* traces in the ionograms (or radio wave scintillations) may not show hemispheric symmetry, being influenced significantly by the local ionospheric conditions. This is first time such evidence (though expected) is available from simultaneous diagnostics of the two irregularity domains.

[31] 3. The evening prereversal enhancement in the vertical drift appears to exercise systematic control on the spread *F*/plasma bubble irregularity development during the COPEX period in such a way that increasing drift velocity is associated with increasing degree of vertical growth of the bubbles under the conditions of generally weak transequatorial winds; it also presents large day-to-day variability.

[32] 4. The evening vertical drift presents a large degree of negative gradient with height, which corresponds to a negative gradient with latitude as well, that is, the vertical plasma drift/zonal electric field decreases with increase of height and latitude. The degree of the gradient (in the decrease) appears to be more marked in the Brazilian longitudes than over Jicamarca for comparable solar flux conditions.

[33] 5. The transequatorial winds were mostly northward during daytime and near midnight hours during the COPEX period. The daytime TEW appears to be significantly underrepresented in the HWM93. There is large day-to-day variability in the TEW which is superimposed on a steady northward increasing trend associated with the progressive displacement from October to December of the subsolar heating region to southern hemisphere.

[34] 6. The magnitude of the TEW as obtained from the hemispheric asymmetry in V_{zp} appear to show general agreement (with some exceptions) with that obtained from the hemispheric asymmetry in h_mF_2 in the evening hours (around 1800–1900 LT), and the northward increase of TEW as part of the seasonal trend also shows general agreement between the two techniques.

[35] 7. Nighttime f_oF_2 increases in the hemisphere which is on the downwind side of the TEW.

[36] 8. There is new evidence in the COPEX data based on case study that the ESF can be suppressed by enhancement (northward in this case) in the TEW.

[37] 9. The degree of medium-term variation in TEW does not appear sufficient enough to dominate over the medium-term variation in the V_{zp} in controlling the observed trend in the ESF occurrence/intensity during the campaign period.

[38] 10. It appears that the magnitude of the TEW increases with increase in magnetic activity during presunrise hours in the present data.

[39] Analysis of the COPEX data is continuing.

[40] **Acknowledgments.** The authors wish to acknowledge support from FAPESP through project 1999/00437-0 and CNPq through grants 502804/2004-1 and 500271/2003-8. B.W.R. was supported by AF grant FA8718-06-C-0072. Logistical support for the operations of the instruments at the conjugate sites (Campo Grande, Cachimbo, and Boa Vista) was provided by the Brazilian Aeronautic Ministry's Instituto Tecnologico de Aeronautic (CTA), which is thankfully acknowledged.

[41] Amitava Bhattacharjee thanks R. Sridharan and another reviewer for their assistance in evaluating this paper.

References

Abdu, M. A. (1997), Major phenomena of the equatorial ionosphere thermosphere system under disturbed conditions, *J. Atmos. Sol. Terr. Phys.*, *59*(13), 1505–1519, doi:10.1016/S1364-6826(96)00152-6.

Abdu, M. A. (2001), Outstanding problems in the equatorial ionosphere-thermosphere electrodynamics relevant to spread F, *J. Atmos. Sol. Terr. Phys.*, *63*, 869–884, doi:10.1016/S1364-6826(00)00201-7.

Abdu, M. A., J. A. Bittencourt, and I. S. Batista (1981a), Some characteristics of spread F at magnetic equatorial station Fortaleza, *J. Geophys. Res.*, *86*, 6836–6842, doi:10.1029/JA086iA08p06836.

Abdu, M. A., J. A. Bittencourt, and I. S. Batista (1981b), Magnetic declination control of the equatorial F region dynamo field development and spread F, *J. Geophys. Res.*, *86*, 11,443–11,446, doi:10.1029/JA086iA13p11443.

Abdu, M. A., R. T. de Medeiros, J. H. A. Sobral, and J. A. Bittencourt (1983a), Spread F plasma vertical rise velocities determined from spaced ionosonde observations, *J. Geophys. Res.*, *88*, 9197–9204, doi:10.1029/JA088iA11p09197.

Abdu, M. A., R. T. de Medeiros, J. A. Bittencourt, and I. S. Batista (1983b), Vertical ionization drift velocities and range spread F in the evening equatorial ionosphere, *J. Geophys. Res.*, *88*, 399–402, doi:10.1029/JA088iA01p00399.

Abdu, M. A., J. H. A. Sobral, P. Richards, M. M. De Gonzalez, Y. N. Huang, B. M. Reddy, K. Cheng, E. P. Szuszcewicz, and I. S. Batista (1996), Zonal/meridional wind and disturbance dynamo electric field control of the low-latitude ionosphere based on the SUNDIAL/ATLAS-1 campaign, *J. Geophys. Res.*, *101*(A12), 26,729–26,740, doi:10.1029/96JA00321.

Abdu, M. A., I. S. Batista, H. Takahashi, J. MacDougall, J. H. Sobral, A. F. Medeiros, and N. B. Trivedi (2003), Magnetospheric disturbance induced equatorial plasma bubble development and dynamics: A case study in Brazilian sector, *J. Geophys. Res.*, *108*(A12), 1449, doi:10.1029/2002JA009721.

Abdu, M. A., I. S. Batista, B. W. Reinisch, J. R. de Souza, E. R. de Paula, J. H. A. Sobral, and T. W. Bullet (2004), Equatorial spread F variability investigations in Brazil: Preliminary results from Conjugate Point Equatorial Experiments Campaign–COPEX, *Eos Trans. AGU*, *85*(17), Jt. Assem. Suppl., Abstract SA43B-06.

Abdu, M. A., I. S. Batista, B. W. Reinisch, J. H. A. Sobral, and A. J. Carrasco (2006a), Equatorial F region evening vertical drift during southern winter months: A comparison of observational data with IRI descriptions, *Adv. Space Res.*, *37*, 1007–1017, doi:10.1016/j.asr.2005.06.074.

Abdu, M. A., K. N. Iyer, R. T. de Medeiros, I. S. Batista, and J. H. A. Sobral (2006b), Thermospheric meridional wind control of equatorial spread F and evening prereversal electric field, *Geophys. Res. Lett.*, *33*, L07106, doi:10.1029/2005GL024835.

Abdu, M. A., P. P. Batista, I. S. Batista, C. G. M. Brum, A. Carrasco, and B. W. Reinisch (2006c), Planetary wave oscillations in mesospheric winds, equatorial evening prereversal electric field and spread F, *Geophys. Res. Lett.*, *33*, L07107, doi:10.1029/2005GL024837.

Abdu, M. A., E. A. Kherani, I. S. Batista, E. R. de Paula, and D. C. Fritts (2009), An evaluation of the ESF/bubble irregularity growth conditions under gravity wave influences based on observational data from the SpreadFEx campaign, *Ann. Geophys.*, in press.

Anderson, D. N., and M. Mendillo (1983), Ionospheric conditions affecting the evolution of equatorial plasma depletions, *Geophys. Res. Lett.*, *10*, 541–544, doi:10.1029/GL010i007p00541.

Anderson, D. N., B. W. Reinisch, C. Valladares, J. Chau, and O. Veliz (2004), Forecasting the occurrence of ionospheric scintillation activity in the equatorial ionosphere on a day-to-day basis, *J. Atmos. Sol. Terr. Phys.*, *66*, 1567–1572, doi:10.1016/j.jastp.2004.07.010.

Bailey, G. J., and N. Balan (1996), Low-latitude ionosphere-plasmasphere model, in *Solar-Terrestrial Energy Program: Handbook of Ionospheric Models*, edited by R. W. Schunk, pp. 173–206, Utah State Univ., Logan.

Batista, I. S., M. A. Abdu, and J. A. Bittencourt (1986), Equatorial F region vertical plasma drifts: Seasonal and longitudinal asymmetries in the American sector, *J. Geophys. Res.*, *91*, 12,055–12,064, doi:10.1029/JA091iA11p12055.

Batista, I. S., M. A. Abdu, A. J. Carrasco, B. W. Reinisch, E. R. de Paula, N. J. Schuch, and F. Bertoni (2008), Equatorial spread F and sporadic E-layer connections during the Brazilian Conjugate Point Equatorial Experiment–COPEX, *J. Atmos. Sol. Terr. Phys.*, *70*, 1133–1143, doi:10.1016/j.jastp.2008.01.007.

Bertoni, F., I. S. Batista, M. A. Abdu, B. W. Reinisch, and E. A. Kherani (2006), A comparison of ionospheric vertical drift velocities measured by Digisonde and incoherent scatter radar at the magnetic equator, *J. Atmos. Sol. Terr. Phys.*, *68*(16), 1851–1852.

Bittencourt, J. A., and M. A. Abdu (1981), A theoretical comparison between apparent and real vertical ionization drift velocities in the equatorial F region, *J. Geophys. Res.*, *86*, 2451–2455, doi:10.1029/JA086iA04p02451.

Bittencourt, J. A., and Y. Sahai (1978), F-region neutral winds from ionosonde measurements of *hmF2* at low latitude magnetic conjugate regions, *J. Atmos. Terr. Phys.*, *40*(6), 669–676, doi:10.1016/0021-9169(78)90124-1.

Burke, W. J., C. Y. Huang, L. C. Gentile, and L. Bauer (2004), Seasonal-longitudinal variability of equatorial plasma bubbles, *Ann. Geophys.*, *22*, 3089–3098.

Cosgrove, R. B., and R. T. Tsunoda (2002), A direction-dependent instability of sporadic-E layers in the nighttime midlatitude ionosphere, *Geophys. Res. Lett.*, *29*(18), 1864, doi:10.1029/2002GL014669.

de Medeiros, R. T., M. A. Abdu, and I. S. Batista (1997), Thermospheric meridional wind at low latitude from measurements of *F* layer peak height, *J. Geophys. Res.*, *102*(A7), 14,531–14,540, doi:10.1029/97JA00799.

Devasia, C. V., et al. (2002), On the possible linkage of thermospheric meridional winds with equatorial spread F, *J. Atmos. Sol. Terr. Phys.*, *64*, 1–12, doi:10.1016/S1364-6826(01)00089-X.

Farley, D. T. (1960), A. theory of electrostatic fields in the ionosphere at nonpolar geomagnetic latitudes, *J. Geophys. Res.*, *65*(3), 869–877, doi:10.1029/JZ065i003p00869.

Farley, D. T., B. B. Balsley, and R. F. Woodman (1970), Equatorial spread *F*: Implications of VHF radar observations, *J. Geophys. Res.*, *75*(34), 7199–7216, doi:10.1029/JA075i034p07199.

Fejer, B. G., E. R. de Paula, S. A. Gonzalez, and R. F. Woodman (1991), Average vertical and zonal *F* region plasma drifts over Jicamarca, *J. Geophys. Res.*, *96*, 13,901–13,906, doi:10.1029/91JA01171.

Fejer, B. G., L. Scherliess, and E. R. de Paula (1999), Effects of the vertical plasma drift velocity on the generation and evolution of equatorial spread *F*, *J. Geophys. Res.*, *104*, 19,859–19,870, doi:10.1029/1999JA900271.

Fritts, D. C., et al. (2008), Gravity wave and tidal influences on equatorial spread F based on observations during the Spread F Experiment (SpreadFEx), *Ann. Geophys.*, *26*, 3235–3252.

Haerendel, G., J. V. Eccles, and S. Cakir (1992), Theory for modeling the equatorial evening ionosphere and the origin of the horizontal plasma flow, *J. Geophys. Res.*, *97*(A2), 1209–1223, doi:10.1029/91JA02226.

Hanson, W. B., and S. Sanatani (1973), Large N_i gradients below the equatorial *F* peak, *J. Geophys. Res.*, *78*, 1167–1173, doi:10.1029/JA078i007p01167.

Hedin, A. E., et al. (1996), Empirical wind model for the upper, middle and lower atmosphere, *J. Atmos. Sol. Terr. Phys.*, *58*, 1421–1447, doi:10.1016/0021-9169(95)00122-0.

Heelis, R. A., P. C. Kendall, R. J. Moffet, D. W. Windle, and H. Rishbeth (1974), Electrical coupling of the *E*- and *F*-regions and its effects on the *F* region drifts and winds, *Planet. Space Sci.*, *22*, 743–756, doi:10.1016/0032-0633(74)90144-5.

Hysell, D. L., and E. Kudeki (2004), Collisional shear instability in the equatorial *F* region ionosphere, *J. Geophys. Res.*, *109*, A11301, doi:10.1029/2004JA010636.

Jyoti, N., C. V. Devasia, R. Sridharan, and D. Tiwari (2004), Threshold height $(h'F)_c$ for the meridional wind to play a deterministic role in the bottomside spread F and its dependence on solar activity, *Geophys. Res. Lett.*, *31*, L12809, doi:10.1029/2004GL019455.

Kelley, M. C. (1989), *The Earth's Ionosphere, Plasma Physics and Electrodynamics*, Academic, San Diego, Calif.

Keskinen, M. J., S. L. Ossakow, and B. G. Fejer (2003), Three-dimensional nonlinear evolution of equatorial ionospheric spread-F bubbles, *Geophys. Res. Lett.*, *30*(16), 1855, doi:10.1029/2003GL017418.

Khmyrov, G. M., I. A. Galkin, A. V. Kozlov, B. W. Reinisch, J. McElroy, and C. Dozois (2008), Exploring Digisonde ionogram data with SAO-X and DIDBase, in *Radio Sounding and Plasma Physics*, *AIP Conf. Proc.*, vol. 974, pp. 175–185, doi:10.1063/1.2885027.

Kil, H., and R. A. Heelis (1998), Global distribution of density irregularities in the equatorial ionosphere, *J. Geophys. Res.*, *103*, 407–417, doi:10.1029/97JA02698.

Kozlov, A., and V. V. Paznukhov (2008), Digisonde drift analysis software, in *Radio Sounding and Plasma Physics*, *AIP Conf. Proc.*, vol. 974, pp. 167–174, doi:10.1063/1.2885026.

Kudeki, E., A. Akgiray, M. Milla, J. L. Chau, and D. L. Hysell (2007), Equatorial spread-F initiation: Post-sunset vortex, thermospheric winds, gravity waves, *J. Atmos. Sol. Terr. Phys.*, *69*, 2416–2427, doi:10.1016/j.jastp.2007.04.012.

MacDougall, J. W., M. A. Abdu, P. T. Jayachandran, J. F. Cecile, and I. S. Batista (1998), Presunrise spread *F* at Fortaleza, *J. Geophys. Res.*, *103*(A10), 23,415–23,425, doi:10.1029/98JA01949.

Maruyama, T. (1988), A diagnostic model for equatorial spread F: 1. Model description and application to electric fields and neutral wind effects, *J. Geophys. Res.*, *93*, 14,611–14,622, doi:10.1029/JA093iA12p14611.

Maruyama, T., and N. Matuura (1984), Longitudinal variability of annual changes in activity of equatorial spread *F* and plasma bubbles, *J. Geophys. Res.*, *89*, 10,903, doi:10.1029/JA089iA12p10903.

Maruyama, T., M. Kawamura, S. Saito, K. Nozaki, H. Kato, N. Hemmakorn, T. Boonchuk, T. Komolmis, and C. H. Duyen (2007), Low latitude ionosphere-thermosphere dynamics studies with ionosonde chain in Southeast Asia, *Ann. Geophys.*, *25*, 1569–1577.

McNamara, L. F., J. M. Retterer, M. A. Abdu, I. S. Batista, and B. W. Reinisch (2008), F2 peak parameters, drifts and spread F derived from

Digisonde ionograms for the COPEX campaign in Brazil, *J. Atmos. Sol. Terr. Phys.*, *70*, 1144–1158, doi:10.1016/j.jastp.2008.02.001.

Mendillo, M., J. Meriwether, and M. Biondi (2001), Testing the thermospheric neutral wind suppression mechanism for day-to-day variability of equatorial spread *F*, *J. Geophys. Res.*, *106*(A3), 3655–3663, doi:10.1029/2000JA000148.

Muella, T. A. H., E. R. de Paula, I. J. Kantor, I. S. Batista, J. H. A. Sobral, M. A. Abdu, K. M. Groves, P. M. Kintner, and P. F. Smorigo (2008), GPS L-band scintillations and ionospheric irregularity zonal drifts inferred at equatorial and low latitude regions, *J. Atmos. Sol. Terr. Phys.*, *70*, 1261–1272, doi:10.1016/j.jastp.2008.03.013.

Nicolls, M. J., M. C. Kelley, M. N. Vlasov, Y. Sahai, P. R. Fagundes, F. Becker-Guedes, and W. L. C. Lima (2006), Observation and modeling of post-midnight uplifts near the magnetic equator, *Ann. Geophys.*, *24*, 1317–1331.

Otsuka, Y., K. Shiokawa, and T. Ogawa (2002), Geomagnetic conjugate observations of equatorial airglow depletions, *Geophys. Res. Lett.*, *29*(15), 1753, doi:10.1029/2002GL015347.

Pingree, J. E., and B. G. Fejer (1987), On the height variation of the equatorial F region vertical plasma drifts, *J. Geophys. Res.*, *92*, 4763–4766, doi:10.1029/JA092iA05p04763.

Prakash, S. (1999), Production of electric field perturbations by gravity wave winds in the *E* region suitable for initiating equatorial spread *F*, *J. Geophys. Res.*, *104*(A5), 10,051–10,069, doi:10.1029/1999JA900028.

Raghavarao, M., Nageswara Rao, J. H. Sastri, G. D. Vyas, and M. Srirama (1988), Role of equatorial ionization anomaly in the initiation of equatorial spread F, *J. Geophys. Res.*, *93*, 5959–5964, doi:10.1029/JA093iA06p05959.

Rastogi, R. G. (1980), Seasonal and solar cycle variations of equatorial spread-F in the American zone, *J. Atmos. Terr. Phys.*, *42*, 593–597, doi:10.1016/0021-9169(80)90093-8.

Reinisch, B. W. (1996), Modern ionosondes, in *Modern Ionospheric Science*, edited by H. Kohl, R. Rüster, and K. Schlegel, Eur. Geophys. Soc., pp. 440–458, Katlenburg-Lindau, Germany.

Reinisch, B. W., M. A. Abdu, I. S. Batista, G. S. Sales, G. Khmyrov, T. A. Bullet, J. Chau, and V. Rios (2004), Multistation Digisonde observations of equatorial spread F in South America, *Ann. Geophys.*, *22*, 3145–3153.

Richmond, A. D., C. Peymirat, and R. G. Roble (2003), Long-lasting disturbances in the equatorial ionospheric electric field simulated with a coupled magnetosphere-ionosphere-thermosphere model, *J. Geophys. Res.*, *108*(A3), 1118, doi:10.1029/2002JA009758.

Rishbeth, H. (1971), Polarization fields produced by winds in the equatorial F region, *Planet. Space Sci.*, *19*, 357–369, doi:10.1016/0032-0633(71)90098-5.

Rishbeth, H., S. Ganguly, and J. C. G. Walker (1978), Field-aligned and field-perpendicular velocities in the ionospheric *F*2-layer, *J. Atmos. Terr. Phys.*, *40*, 767–784, doi:10.1016/0021-9169(78)90028-4.

Saito, S., and T. Maruyama (2006), Ionospheric height variations observed by ionosondes along magnetic meridian and plasma bubble onsets, *Ann. Geophys.*, *24*, 2991–2996.

Sales, G., B. Reinisch, J. Scali, C. Dozois, T. Bullett, E. Weber, and P. Ning (1996), Spread *F* and the structure of equatorial ionization depletions in the southern anomaly region, *J. Geophys. Res.*, *101*(A12), 26,819–26,827, doi:10.1029/96JA01946.

Sastri, J. H., M. A. Abdu, I. S. Batista, and J. H. A. Sobral (1997), Onset conditions of equatorial (range) spread *F* at Fortaleza, Brazil, during the June solstice, *J. Geophys. Res.*, *102*(A11), 24,013–24,021, doi:10.1029/97JA02166.

Scali, J. L., B. W. Reinisch, C. J. Heinselman, and T. Bullett (1995), Coordinated Digisonde and incoherent scatter radar *F* region drift measurements at Sondre Stromfjord, *Radio Sci.*, *30*, 1481–1498, doi:10.1029/95RS01730.

Scherliess, L., and B. G. Fejer (1999), Radar and satellite global equatorial F region global equatorial F region vertical drift model, *J. Geophys. Res.*, *104*, 6829–6842, doi:10.1029/1999JA900025.

Sekar, R., and R. Raghavarao (1995), Critical role of the equatorial topside F region on the evolutionary characteristics of the plasma bubbles, *Geophys. Res. Lett.*, *22*(23), 3255–3258, doi:10.1029/95GL03078.

Sobral, J. H. A., and M. A. Abdu (1990), Latitudinal gradient in the plasma bubble zonal velocities as observed by scanning 630-nm airglow measurements, *J. Geophys. Res.*, *95*(A6), 8253–8257, doi:10.1029/JA095iA06p08253.

Sobral, J. H. A., M. A. Abdu, H. Takahashi, M. J. Taylor, E. R. de Paula, C. J. Zamlutti, and G. L. Borba (2002), Ionospheric plasma bubble climatology over Brazil based on 22 years (1977–1998) of OI 630 nm airglow observations, *J. Atmos. Sol. Terr. Phys.*, *64*(12–14), 1517–1524, doi:10.1016/S1364-6826(02)00089-5.

Sobral, J. H. A., et al. (2009), Ionospheric zonal velocities at conjugate points over Brazil during the COPEX campaign: Experimental observations and theoretical validations, *J. Geophys. Res.*, *114*, A04309, doi:10.1029/2008JA013896.

Souza, J. R., M. A. Abdu, I. S. Batista, and G. J. Bailey (2000), Determination of vertical plasma drift and meridional wind using the Sheffield University Plasmasphere Ionosphere Model and ionospheric data at equatorial and low latitudes in Brazil: Summer solar minimum and maximum conditions, *J. Geophys. Res.*, *105*(A6), 12,813–12,821, doi:10.1029/1999JA000348.

Sridharan, R., D. Pallam Raju, R. Raghavarao, and P. S. V. Rao (1994), Precursor to equatorial spread-*F* in the OI 630.0 nm dayglow, *Geophys. Res. Lett.*, *21*, 2797–2800, doi:10.1029/94GL02732.

Su, S.-Y., C. K. Chau, and C. H. Liu (2008), On monthly/seasonal/longitudinal variation of equatorial irregularity occurrences and their relationship with the postsunset vertical drift velocities, *J. Geophys. Res.*, *113*, A05307, doi:10.1029/2007JA012809.

Sultan, P. J. (1996), Linear theory and modeling of the Rayleigh-Taylor instability leading to the occurrence of equatorial spread *F*, *J. Geophys. Res.*, *101*, 26,875–26,891, doi:10.1029/96JA00682.

Thampi, S. V., S. Ravindran, T. K. Pant, C. V. Devasia, P. Sreelatha, and R. Sridharan (2006), Deterministic prediction of post-sunset ESF based on the strength and asymmetry of EIA from ground based TEC measurements: Preliminary results, *Geophys. Res. Lett.*, *33*, L13103, doi:10.1029/2006GL026376.

Tsunoda, R. T. (1981), Time evolution and dynamics of equatorial backscatter plumes: 1. Growth phase, *J. Geophys. Res.*, *86*, 139–149, doi:10.1029/JA086iA01p00139.

Tsunoda, R. T. (1985), Control of the seasonal and longitudinal occurrence of equatorial scintillations by the longitudinal gradient in integrated *E* region Pedersen conductivity, *J. Geophys. Res.*, *90*, 447–456, doi:10.1029/JA090iA01p00447.

Tsunoda, R. T. (2007), Seeding of equatorial plasma bubbles with electric fields from and E_s-layer instability, *J. Geophys. Res.*, *112*, A06304, doi:10.1029/2006JA012103.

Tsunoda, R. T. (2008), Satellite traces: An ionogram signature for large-scale wave structure and a precursor for equatorial spread *F*, *Geophys. Res. Lett.*, *35*, L20110, doi:10.1029/2008GL035706.

Valladares, C. E., S. Basu, K. Groves, M. P. Hagan, D. Hysell, A. J. Mazella Jr., and R. E. Sheehan (2001), Measurement of the latitudinal distributions of total electron content during equatorial spread *F* events, *J. Geophys. Res.*, *106*, 29,133–29,152, doi:10.1029/2000JA000426.

Woodman, R. F., and C. LaHoz (1976), Radar observations of *F* region equatorial irregularities, *J. Geophys. Res.*, *81*, 5447–5466, doi:10.1029/JA081i031p05447.

Zalesak, S. T., S. L. Ossakow, and P. K. Chaturvedi (1982), Nonlinear equatorial spread *F*: The effect of neutral winds and background Pedersen conductivity, *J. Geophys. Res.*, *87*, 151–166, doi:10.1029/JA087iA01p00151.

M. A. Abdu, I. S. Batista, E. R. de Paula, J. R. de Souza, and J. H. A. Sobral, Instituto Nacional de Pesquisas Espaciais, Avenue dos Astronautas 1578, São José dos Campos, SP 12201-970, Brazil. (maabdu@dae.inpe.br)

K. M. Groves and T. R. Pedersen, Air Force Research Laboratory, AFRL/VSBXI, 29 Randolph Road, Hanscom AFB, MA 01731-3010, USA.

A. F. Medeiros, Universidade Federal de Campina Grande, Ave Aprigio Veloso 882, Campina Grande, 58.109.970, PB, Brazil.

B. W. Reinisch, Center for Atmospheric Research, University of Massachusetts, 600 Suffolk Street, Lowell, MA 01854, USA.

N. J. Schuch, Centro Regional Sul de Pesquisas Espaciais, INPE, Cidade Universitaria, Santa Maria, 97110-970, RS, Brazil.